Open access • Posted Content • DOI:10.1101/2021.05.12.442687

RTK-dependent inducible degradation of mutant PI3K alpha drives GDC-0077 (Inavolisib) efficacy — Source link

Kyung Song, Kyle A. Edgar, Emily J. Hanan, Marc Hafner ...+23 more authors

Institutions: Genentech

Published on: 13 May 2021 - bioRxiv (Cold Spring Harbor Laboratory)

Topics: PI3K/AKT/mTOR pathway, Receptor tyrosine kinase, P110α and Mutant

1 **RTK-dependent inducible degradation of mutant PI3Kα drives GDC-0077 (Inavolisib)**
2 **efficacy**
3

4 Kyung W. Song[1+], Kyle A. Edgar[9+], Emily J. Hanan[2], Marc Hafner[4], Jason Oeh[7],
5 Mark Merchant[7], Deepak Sampath[7], Michelle A. Nannini[7], Rebecca Hong[7], Lilian Phu[3], William
6 F. Forrest[4], Eric Stawiski[4], Stephen Schmidt[8], Nicholas Endres[8], Jane Guan[1], Jeffrey J. Wallin[7#],
7 Jonathan Cheong[6], Emile Plise[6], Gail Philips[1], Laurent Salphati[6], Timothy P. Heffron[2], Alan
8 Olivero[2], Shiva Malek[1], Steven T. Staben[2], Donald S. Kirkpatrick[3], Anwesha Dey[1]*, Lori S.
9 Friedman[9]*
10
11 **Affiliations:** Departments of Discovery Oncology[1], Discovery Chemistry[2], Microchemistry,
12 Proteomics & Lipidomics[3], Bioinformatics[4], Structural Biology[5], Drug Metabolism and
13 Pharmacokinetics[6], Translational Oncology[7], and Biochemical and Cell Biology[8],Genentech,
14 Inc., 1 DNA Way, South San Francisco, California 94080, USA
15 [+] These authors contributed equally
16 * Corresponding authors
17 Anwesha Dey, PhD and Lori S. Friedman, PhD
18 Department of Discovery Oncology
19 Genentech, Inc.
20 1 DNA Way, MS 41-1a, South San Francisco, CA 94080
21 E-mail: dey.anwesha@gene.com; friedman.lori@gmail.com
22 [9]Current address: Oric Pharmaceuticals 240 E. Grand Ave, Fl2 South San Francisco, CA 94080,
23 USA

Abstract

PIK3CA is one of the most frequently mutated oncogenes; the p110α protein it encodes plays a central role in tumor cell proliferation and survival. Small molecule inhibitors targeting the PI3K p110α catalytic subunit have entered clinical trials, with early-phase GDC-0077 (Inavolisib) studies showing anti-tumor activity and a manageable safety profile in patients with *PIK3CA*-mutant, hormone receptor-positive breast cancer as a single agent or in combination therapy. Despite this, preclinical studies have shown that PI3K pathway inhibition releases negative feedback and activates receptor tyrosine kinase signaling, reengaging the pathway and attenuating drug activity. Here we discover that GDC-0077 and taselisib more potently inhibit mutant PI3K pathway signaling and cell viability through unique HER2-dependent degradation. Both are more effective than other PI3K inhibitors at maintaining prolonged pathway suppression, resulting in enhanced apoptosis and greater efficacy. This unique mechanism against mutant p110α reveals a new strategy for creating inhibitors that specifically target mutant tumors with selective degradation of the mutant oncoprotein and also provide a strong rationale for pursuing PI3Kα degraders in patients with HER2-positive breast cancer.

Keywords: GDC-0077 (Inavolisib), taselisib, breast cancer, HER2-positive, *PIK3CA*, PI3K, p110α

Introduction

Oncogenic mutations in the *PIK3CA* gene increase lipid kinase activity and transform cells (Isakoff et al., 2005; Kang et al., 2005; Samuels et al., 2005). The alpha isoform of PI3K is a dimer

47 composed of the p110α catalytic subunit and a p85 regulatory subunit which functions to stabilize
48 p110α and reduce kinase activity (Yu et al., 1998). The binding of a phosphorylated receptor
49 tyrosine kinase (RTK) activates p110α through the release of a subset of inhibitory contacts with
50 p85 (Burke and Williams, 2013). Common hotspot mutations in *PIK3CA* helical (*E542K*, *E545K*)
51 and kinase (*H1047R*) domains function by perturbing local interfaces between p85 and p110α
52 (Echeverria et al., 2015; Miled et al., 2007) and increasing dynamic events required for catalysis
53 on membranes (Burke et al., 2012). Several inhibitors of PI3K have entered clinical trials, yet in
54 patients with *PIK3CA*-mutant tumors the efficacy has been modest, in part due to a limited
55 therapeutic index (Krop et al., 2016; Martin et al., 2017; Mayer et al., 2017; Rodon et al., 2013).
56 Hence, we reasoned that it might be possible to improve the therapeutic index by identifying
57 compounds with increased specificity for mutant p110α.
58

59 **Results**

60 **PI3K inhibitor potency in *PIK3CA*-mutant cells**

61 A selection of PI3K inhibitors were profiled for biochemical activity and pharmacokinetic
62 properties, including inhibitors across several chemical classes and with varying p110 isoform
63 selectivity (Figure 1A). Taselisib and GDC-0077 showed increased mutant potency in cell viability
64 assays in a cancer cell line panel compared with other PI3K inhibitors (including the alpha isoform-
65 selective inhibitor, BYL719) (Figure 1B). Furthermore, taselisib (and later, GDC-0077) was a
66 stronger inducer of cell death compared with other compounds, specifically in *PIK3CA*-mutant
67 cancer cell lines (Figure S1A), suggesting that taselisib is more potent in *PIK3CA*-mutant cells
68 compared with to other PI3K inhibitors. We compared PI3K inhibitor potencies in parental
69 isogenic SW48 colon cancer cells bearing wild-type (WT) *PIK3CA* and matched isogenic lines

70 expressing *H1047R* or *E545K* hotspot mutants knocked into one allele of the *PIK3CA* locus.
71 Taselisib potency (half maximal effective concentration [EC_{50}]) increased 3-fold in *PIK3CA*-
72 mutant cells versus parental WT SW48 cells, while GDC-0941 (Folkes et al., 2008) displayed
73 comparable EC_{50} in mutant and WT cells (Figure 1C). To assess whether this potency shift was
74 correlated with the taselisib chemical scaffold, structurally related analogs with increased alpha-
75 isoform specificity, GNE-102 and GNE-326 (Heffron et al., 2016), and a PI3Kα inhibitor from an
76 unrelated chemical class (BYL719) (Furet et al., 2013) were assessed and found to not have a
77 potency differential in mutant versus WT isogenic cells (Figure S1B). We also confirmed that
78 inhibition of multiple PI3K isoforms did not play a role in this increased potency. Taselisib binds
79 equipotently to p110α and p110δ isoforms but is selective against p110β and p110γ isoforms
80 (Figure 1A). However, combination of a p110α inhibitor (GNE-102) with a p110δ inhibitor
81 (idelalisib) (Sadhu et al., 2003) did not impact cell potency, nor did the combination of taselisib
82 with a p110β inhibitor (TGX-221) (Jackson et al., 2005) (Figures S1C and S1D). Neither cell
83 permeability differences nor intracellular accumulation of inhibitors could explain the increased
84 potency of taselisib in mutant cells (Figure S1E).
85
86 ***In vivo* efficacy of GDC-0077**
87 We next asked whether this greater potency and enhanced cell death manifested *in vivo* in
88 mutant PI3K tumor xenografts. Indeed, we observed greater efficacy for taselisib and GDC-0077
89 compared with a maximum tolerated dose (MTD) of BYL719 (Figure 1D). In addition, GDC-0077
90 treatment at the MTD *in vivo* resulted in tumor regressions in multiple *PIK3CA*-mutant xenograft
91 and patient-derived xenograft models (HCC1954, KPL4, and HCI-003 PDX) (Figures S1F).

92 Given the potency of GDC-0077 and the significant improvement in PI3Kα isoform
93 selectivity over both taselisib and BYL719 (Figures 1A and 1B), we next evaluated the efficacy of
94 GDC-0077 and the suitability for combination with standard of care in hormone receptor (HR)-
95 positive/HER2-negative breast cancers. These included aromatase inhibitors and, more recently,
96 CDK4/6 inhibitors such as palbociclib. We therefore assessed the effect of combining GDC-0077
97 with these drugs to evaluate efficacy and safety. First, we measured *in vitro* growth of five
98 *PI3KCA*-mutant HR-positive lines across different concentrations of GDC-0077 with or without
99 E2 (to mimic aromatase inhibitors [AIs]) and with or without 0.15 μM of palbociclib. To assess
100 growth, endpoint cell population, as measured by CyQuant assay, was normalized to the cell
101 population at the time of treatment using the growth-rate inhibition (GR) method (Hafner et al.,
102 2016). A GR value of 1 meant no inhibition, 0 meant no net growth, and negative values
103 represented cell loss. Response in *PIK3CA E545K*-mutant MCF-7 cells showed that addition of
104 GDC-0077 induced a strong cytotoxic response in all combination treatments, as reflected by
105 negative GR values for concentrations of 0.12μM and above (Hafner et al., 2016) (Figure 2A).
106 When assessing the efficacy of the combination treatments across all five cell lines, we found that
107 the GR values measured in the condition with palbociclib and without E2 (equivalent to AI)
108 decreased by a median of 0.25 when adding 0.123 μM of GDC-0077, showing a broad increase in
109 efficacy by combining GDC-0077 with standard of care treatments (Figure 2B and S2A).
110 We then sought to validate this increased efficacy *in vivo*. Palbociclib (50 mg/kg) combined
111 with fulvestrant (200mg/kg) only conferred tumor growth inhibition (TGI) of 71%, whereas
112 addition of GDC-0077 (25 mg/kg) further reduced tumor burden (mean TGI of 106%, N = 12,
113 Figure 2C), consistent with the response observed *in vitro* (Figure 2A). Weight loss was modest at
114 8.1% in the triple combination cohort (Figure S2B), suggesting tolerability of adding GDC-0077

115 to a regimen with endocrine therapy plus CDK4/6 inhibitors. Similar efficacy results were obtained
116 with taselisib combined with palbociclib (Figure S2C), although weight loss was higher (Figure
117 S2C) with taselisib as expected. Also, taselisib could only be combined with palbociclib and not
118 the triple combination. Taken together, these data suggested the possibility of combining GDC-
119 0077 with both palbociclib and fulvestrant for superior efficacy in *PIK3CA*-mutant, *HER2*-
120 negative tumors and providing a therapeutic window not achievable with earlier PI3K inhibitors.
121

122 **Taselisib and GDC-0077 induce mutant p110α degradation**

123 In order to determine the mechanistic basis for this efficacy differential in *PIK3CA*-mutant
124 tumors, we compared the effects downstream (pAKT) and upstream (pHER3) of PI3K signaling
125 for GDC-0077 versus BYL719 over a timecourse. In both cases we observed robust acute
126 inhibition of pAKT treatment; however, GDC-0077 demonstrated sustained inhibition of pAKT
127 over the 24-hour treatment time despite inducing release of negative feedback, as measured by
128 upregulation of pHER3 (as is also observed for BYL719) (Figure 3A).

129 We reasoned that one possible mechanism of enabling of sustained inhibition of pAKT in
130 spite of elevated pHER3 levels would be via drug-induced sequestration of PI3K away from the
131 plasma membrane. In order to investigate this hypothesis, levels of p110α protein in sub-cellular
132 fractions were evaluated by western blot at various timepoints after taselisib treatment.
133 Unexpectedly, we discovered time-dependent p110α protein depletion from the *PIK3CA*-mutant
134 cells following taselisib treatment, regardless of the subcellular fraction evaluated (Figure S3A).
135 BYL719 did not significantly impact p110α protein levels. Comparing whole cell lysates from
136 *PIK3CA*-mutant and -WT breast cancer cells by western blot, taselisib treatment for 8 hours caused
137 the dose-dependent depletion of p110α protein specifically in *PIK3CA H1047R*-mutant HCC1954

138 cells. No significant change was observed for p110α in *PIK3CA*-WT HDQ-P1 cells (Figure S3B).
139 Treatment with BYL719 did not affect p110α levels in any cell lines tested. Transcription of
140 *PIK3CA* alleles was not diminished following taselisib treatment (Figure S3C), implicating post-
141 transcriptional regulation of mutant p110α protein.

142 We investigated p110α protein depletion in p110α mutant xenograft breast cancer models
143 and found that membrane-associated p110α was depleted 4 hours after a single oral dose of 15
144 mg/kg taselisib in individual tumors from a p110α-mutant HCC1954 xenograft model, and that
145 p110α depletion was not observed with 40 mg/kg BYL719 (Figure S3D). In the same xenograft
146 model, a single oral dose of 50 mg/kg GDC-0077 depleted p110α protein expression for up to 8
147 hours, further confirming a similar mechanism of action for both taselisib and GDC-0077. In
148 Phase Ia clinical trials, taselisib and GDC-0077 had antitumor activity in *PIK3CA*-mutant tumors
149 as assessed by response rates (Juric et al., 2017). The free drug exposures achieved in the clinic
150 were evaluated in tissue culture experiments with *PIK3CA* mutant breast cancer lines. Unlike
151 pictilisib (GDC-0941), both taselisib (GDC-0032) and inavolisib (GDC-0077) treatment for 24
152 hours resulted in p110α degradation at clinically relevant concentrations (Figure S4A).

153 To generate direct evidence that taselisib or GDC-0077 treatment was preferentially
154 depleting mutant p110α protein within a mixed WT and mutant allelic population, we took
155 advantage of a neo-tryptic peptide encoded by the *H1047R* mutation to assess p110α protein levels
156 by mass spectrometry. HCC1954 parental cells expressing both mutant and WT p110α were
157 treated with taselisib for 24 hours, revealing loss of the mutant specific peptide only in the taselisib-
158 treated sample, p=0.00016 (Figure 3B). There was no significant change in WT p110α, while the
159 total p110α pool decreased commensurate with the initial abundance of the mutant protein (Figure
160 S4B). Similarly, depletion of the E545K mutant protein was observed in HCC202 heterozygous

161 cells, as shown by assaying a second mutant specific neo-tryptic peptide at this locus, p=0.032
162 (Figure S4C).

163 To further explore the molecular mechanisms underlying inhibitor-induced mutant p110α
164 depletion, we examined whether reduction of p110α could be attributed to degradation. A
165 proteasome inhibitor, MG132, and a ubiquitin-activating enzyme E1 inhibitor both rescued the
166 p110α degradation induced by taselisib and GDC-0077 (Figure 3C), while lysosomotropic agents
167 failed to do so (Figure S4D). We next employed ubiquitin pull down assays to confirm that mutant
168 p110α is inducibly ubiquitinated upon taselisib treatment, and that this signal further accumulated
169 when cells were co-treated with MG132 to prevent proteasomal degradation of ubiquitinated
170 p110α (Figure 3D). Accordingly, no ubiquitinated p110α was detected in cells treated with UAE1
171 inhibitor (Figure 3D). Importantly, taselisib also induced ubiquitination and degradation of E545K
172 p110α in the HCC202 cell model, with comparable rescue by MG132 and UAE1 inhibition (Figure
173 3D).

174 Visualization of p110α depletion on western blot was more easily discerned in HCC1954
175 cells, which have an increased copy number of the mutant *p110α* allele. Quantitative Reverse
176 Transcription PCR (qRT-PCR) analysis confirmed higher expression of the mutant allele (Figure
177 S4E). In order to generate a clean system to better compare differential effect of inhibitors on WT
178 and mutant p110alpha, we used CRISPR/cas9 to generate isogenic HCC1954 cell lines bearing
179 either the *H1047* WT allele or the mutant *H1047R* allele, named HCC1954_mutant and
180 HCC1954_WT (Figure S4E). Taselisib treatment resulted in ubiquitination and depletion of p110α
181 protein only in the HCC1954_mutant cells, and not in the matched HCC1954_WT cells (Figure
182 3E and Figure S4F).

183 Since the basal level of ubiquitination was significantly higher for membrane-bound
184 mutant p110α compared with WT p110α (Figure S4G), we hypothesized that the mutant p110α
185 protein may be inherently less stable than the WT protein, as previously noted for mutant EGFR
186 (Greig et al., 2015). Consistent with prior literature (Yu et al., 1998), pulse-chase experiments in
187 HCC1954_WT isogenic cells indicated a protein half-life for WT p110α of ~26.7 hours. In
188 contrast, the H1047R mutant protein half-life was ~9.6 hours in the basal state, and was further
189 shortened to ~4 hours upon treatment with taselisib (Figure 3F). Together these data demonstrate
190 that mutant p110α oncoprotein is inherently less stable and more vulnerable to inhibitor-mediated
191 degradation in a ubiquitin and proteasome dependent manner.
192
193 **p85β potentiates p110α degradation by recruiting p110α to the membrane**
194 It has previously been shown that p110α/p85 dimers are activated by growth factor-
195 stimulated RTK signaling (Cantley et al., 1991). The mechanism of this activation involves release
196 of inhibitory contacts between p110 and p85 once bound to phosphotyrosine residues of an RTK
197 (Backer, 2010; Burke and Williams, 2013). We next reasoned that the ability of our small molecule
198 degraders to accelerate the turnover of activated mutant protein might be through appropriation of
199 the p110α activation process. In support of this hypothesis, cell fractionation studies showed that
200 taselisib-inducible ubiquitination of p110α occurred preferentially in the membrane fraction
201 (Figure 4A).
202 One major effector that recruits p110α to RTK is the p85 PI3K regulatory subunit. There
203 are three p85 isoforms in class 1A PI3K: p85α, p85β, and p55γ. We first confirmed comparable
204 expression levels of all three isoforms in HCC1954 cells (Figure S5A). By co-immunoprecipitation
205 we also demonstrated that all three isoforms interact with mutant p110α (Figure S5A). We next

206 evaluated the effect of p85 isoforms on inhibitor-induced p110α degradation. Knockdown of both
207 p85α and p55γ showed similar levels of taselisib-induced p110α degradation compared with
208 control siRNA-treated cells. In contrast, we observed that p85β KD rescued taselisib-mediated
209 p110α degradation (Figure 4B). We further observed that p85β KD resulted in inhibition of
210 pathway signaling, shown by reduced pAKT levels. These data suggest that p85 isoforms do not
211 have redundant roles and that the p85β, but not the p85α or p55γ isoforms is involved in mutant
212 p110α degradation. Reduced pAKT levels with p85β KD is most likely a result of reduced p110α
213 membrane localization.

214 This observation also suggested that p85 isoforms have differential affinity for RTK
215 interaction. To address this question, we next performed a series of co-immunoprecipitation
216 experiments. p85α or p85β were immunoprecipitated from the membrane fraction and
217 immunoblotted with several antibodies, including four receptors that are highly activated in
218 HCC1954 cells (Figure S5B). Both p85α and p85β interacted with p110α, consistent with previous
219 results. We also observed a stronger association between p85β and HER2 and HER3 than observed
220 for p85α or p55γ protein (Figure 4C, Figure S5C). We could not detect an interaction between p85
221 isoforms with EGFR or c-MET under these conditions.

222 To further confirm this observation, we next tested whether inhibition of HER2
223 phosphorylation blocked p85β binding to HER2 and rescue p110α degradation. Cells were treated
224 with taselisib or lapatinib alone or in combination for various timepoints. These cell lysates were
225 next immunoprecipitated using p85α or p85β antibody and immunoblotted with HER2 and HER3
226 antibodies. In taselisib-treated cells, strong interaction between p85β and HER2/3 was observed.
227 Treatment with lapatinib blocked this interaction, confirming that activated HER2 contributes to
228 p85β membrane binding (Figure S5D). These results further demonstrated that p85β plays an

229 important role in recruiting p110α to the membrane, and that this is likely through binding to
230 activated HER2 and HER3.

231 To further confirm the role of p85β in p110α degradation, we next tested the effects of p85
232 knockdown on K63 and K48 polyubiquitin chain formation on p110α. Upon knockdown of p85α
233 or p85β and following inhibitor treatment, K63 or K48 ubiquitin conjugated proteins were
234 immunoprecipitated using linkage specific antibodies and immunoblotted with p110α. In both
235 control- and p85α-depleted cells, taselisib treatment induced both K63 and K48 linked
236 ubiquitination on p110α. However, upon p85β depletion, ubiquitination of p110α was no longer
237 detected (Figure 4D). These data further confirm that the p85β regulatory subunit plays an
238 important role in taselisib-induced mutant p110α degradation, by recruiting p110α to the
239 membrane where ubiquitination occurs.

240

241 **Taselisib- and GDC-0077-induced mutant p110α degradation is dependent on RTK activity**

242 To further understand whether inhibitor-induced mutant p110α degradation is dependent
243 on its recruitment to activated RTK, we next investigated the efficacy of the two clinically relevant
244 molecules, GDC-0077 and BYL719 (Alpelisib). Unexpectedly, we observed a significant
245 difference in the sensitivity of *HER2*-amplified (~20-fold difference between the mean IC^{50} values)
246 versus *HER2*-negative cell lines (~6-fold difference between two inhibitors) to GDC-0077 versus
247 BYL719. The inhibitors were not differentiated in WT cell lines regardless of *HER2* status (Figure
248 5A). These data imply that RTK activity may define the sensitivity of a cell line to inducible
249 degradation of mutant-p110α. To confirm this finding, a panel of over 50 cell lines harboring
250 *PIK3CA* hot spot mutations were analyzed (Figure 5B). Most of these were heterozygous, carrying
251 both WT and mutant *PIK3CA* alleles at differing frequencies. For easier visualization of mutant

252 p110α depletion, we analyzed the cell lines with higher copy numbers of mutant alleles that also
253 represented each hot spot mutation across various tumors (Figure 5B, colored in blue). In a cell
254 proliferation assay, these cell lines have varying GDC-0077 sensitivity. All of the selected
255 representative cell lines responded to GDC-0077, as measured by inhibition of pAKT. Not all cell
256 lines showed visible p110α degradation; those that showed mutant p110α degradation were
257 HCC2185, HCC1954, MDAMB453, and KPL4 (Figure 5B). It was particularly striking that all
258 *HER2*-amplified cell lines showed p110α degradation. In contrast, the *HER2*-negative cell lines
259 were resistant to degradation except HCC2185. To further understand this observation, we tested
260 if activating RTK by addition of growth factors would induce p110α degradation. A subset of
261 *HER2*-negative cell lines, each harboring WT or one of three p110α hot spot mutations, were
262 treated with GDC-0077 alone or in combination with growth factors. All responded to growth
263 factors, as shown by induction of HER3 phosphorylation. Consistent with our data, p110α levels
264 did not decrease in *HER2*-negative cell lines treated with GDC-0077 alone. However, the
265 combination of growth factors and GDC-0077 induced p110α degradation in all three p110α-
266 mutant lines. WT p110α protein expression was not affected by addition of growth factors (Figure
267 5C). Immunoprecipitation and pull down of p110α revealed that p110α degradation was markedly
268 delayed when RTK interaction with the p110α/p85 complex was disrupted, with limited inducible
269 degradation observed at the 8 hr timepoint (Figure 5D, upper panel). Conversely, inhibition of
270 RTK phosphorylation by lapatinib partially rescued taselisib-mediated p110α degradation in
271 HCC1954 cells (Figure 5D, lower panel). Similar to taselisib, GDC-0077-induced mutant p110α
272 degradation was rescued by lapatinib treatment (Figure 5E). In support of these results, we
273 observed that in multiple patient derived xenograft (PDX) models, high basal pHER2 and pHER3
274 expression level correlated with better taselisib-mediated p110α degradation, with weaker

275 degradation observed in tumors with low levels of pRTK (Figure S6A). In addition, within this
276 group of PDX models, the degree of degradation appeared to correlate with basal pRTK
277 expression. Taken together, our data support a model where small molecule-induced p110α mutant
278 degradation depends on RTK activity in *PIK3CA* mutant cancers.
279

280 **p110α-mutant degrading inhibitors provide more sustained benefit in HER2-positive versus**
281 **HER2-negative p110α-mutant cancers**

282 Given that RTK reactivation could potentially limit efficacy, we also aimed to understand
283 activity in HER2-positive breast cancers. Degradation of mutant p110α blocked the feedback
284 induced pathway reactivation and resulted in enhanced potency of taselisib and GDC-0077 in
285 cellular assays and an increase in apoptosis in mutant cells. Our data thus far predict that drugs
286 which induce degradation of mutant p110α may show more sustained benefit over non-degraders
287 by preventing pathway reactivation. We speculated that the extent of negative feedback depends
288 on the amount of RTK expression, implying that inhibitor-mediated feedback pathway reactivation
289 would be weak in *HER2*-negative cells. Also, based on our findings, low RTK activity may result
290 in inefficient mutant p110α degradation.Pathway reactivation was not observed in *HER2*-negative
291 cells, in contrast to *HER2*-amplified cells, irrespective of the inhibitors used. This suggests that in
292 *HER2*-negative mutant cells, the degrader mechanism of action may not provide additional benefit
293 over drugs with a non-degrader mechanism (model in Figure 6A). This was further confirmed in
294 a panel of *PIK3CA* mutant cell lines. In *HER2*-amplified cells, GDC-0077 resulted in sustained
295 pathway inhibition, while BYL719 activity was attenuated, as evidenced by rebound of pAKT
296 levels (Figure S6B). In contrast, in a panel of *HER2*-negative lines, there was no difference in
297 pathway inhibition by both inhibitors, GDC-0077 or BYL719.

298 Based on these data, we posited that we could best leverage the degradation potential of
299 GDC-0077 in *HER2*-amplified cancers. In HER2-driven breast cancers, HER2-targeted therapy is
300 the standard of care. However, *HER2*-amplified tumors with p110α mutations are less responsive
301 to HER2-targeted therapy. Therefore, combination treatment of the PI3K pathway inhibitors and
302 HER2 targeted therapy should result in enhanced efficacy. Indeed, combination of HER2
303 inhibitors, trastuzumab and pertuzumab, in combination with taselisib in a HER2-positive mutant
304 p110α KPL-4 xenograft model showed better response compared with single drugs alone (Figure
305 6B. Furthermore, combining ado-trastuzumab emtansine (TDM-1) with GDC-0077 showed a
306 synergistic effect in the KPL-4 xenograft model as well (Figure 6C).

307 Given that most p110α-mutant cells are heterozygous, selective mutant p110α degradation
308 would imply a possible scenario where WT p110α protein is still present and can reactivate the
309 same pathway and dampen inhibitor activity (Figure S6C). To test this possibility, we compared
310 levels of feedback reactivation in an engineered homozygous versus heterozygous line. In a
311 HCC1954 WT homozygous isogenic line, the pathway was reactivated by both GDC-0077
312 (degrader) and BYL719 (non-degrader), as expected (Figure S6D). In a HCC1954 mutant
313 homozygous isogenic line, BYL719, but not GDC-0077 treatment reactivated pathway signaling.
314 Importantly, when compared, the phenotype of a heterozygous parental line behaved similar to
315 that of a p110α mutant homozygous line, suggesting that in heterozygous cells, mutant p110α
316 functions as the main driver of cell signaling (Figure S6D). Furthermore, cell proliferation assays
317 mirrored the inhibitor efficacy as well. GDC-0077 showed the same efficacy between homozygous
318 and heterozygous mutant lines but showed reduced efficacy in WT isogenic lines (Figure S6D),
319 while no shift in IC_{50} was observed between all lines following BYL719 treatment. To further
320 confirm these results, the same experiment was performed in *HER2*-negative lines. Consistent with

321 our hypothesis for the role of HER2 in pathway reactivation, feedback pathway reactivation was
322 not detected even in a homozygous WT line upon treatment with GDC-0077 or BYL719. In cell
323 viability assays, neither inhibitor showed a shift in efficacy between isogenic lines (Figure S6E).
324 Taken together, our data demonstrate that degradation potential of GDC-0077 would be most
325 leveraged in HER2-positive breast cancers for more sustained pathway inhibition.
326

327 **Discussion**

328 In summary, we have discovered that the mutant p110α oncoprotein has unique
329 characteristics compared with WT p110α: a shorter half-life, ubiquitination in the membrane
330 fraction, and proteasome-mediated turnover. Furthermore, the mutant oncoprotein is susceptible
331 to increased proteasome-mediated degradation upon binding particular PI3K inhibitors such as
332 taselisib and GDC-0077. Our results suggest that RTK activity plays a key role in regulating
333 p110α degradation by recruiting p110α to the membrane. The mutant oncoprotein may be
334 particularly vulnerable to additional local conformational changes that impact membrane binding,
335 and taselisib and GDC-0077 may be enhancing this effect to accelerate proteasome-mediated
336 degradation. This discovery reveals a new mechanism of action to exploit in *PIK3CA*-mutant
337 tumors, opening an exciting path to increasing drug efficacy for the predominant oncogene in
338 cancer. With a combined mutant-p110α degrader mechanism and exquisite p110α isoform
339 selectivity, the PI3Kα-selective inhibitor and mutant PI3Kα degrader GDC-0077 may provide
340 opportunities for previously inaccessible combination therapy with greater clinical responses.
341 Moreover, this suggests that it may be possible to exploit endogenous mechanisms and the intrinsic
342 instability of mutant oncoproteins more broadly to develop tumor-selective therapeutic agents.
343 Based on these mechanistic discoveries, it may be possible to create efficacious compounds that

344 specifically deplete the mutant p110α protein without blocking WT PI3K signaling, similar to
345 engineered mouse models of cancer in which removal of the mutant *PIK3CA* oncogene induces
346 regressions in the presence of WT PI3K (Cheng et al., 2016; Engelman et al., 2008). For the over
347 2 million cancer patients diagnosed annually with *PIK3CA*-mutant tumors, this discovery opens
348 the possibility of a future therapeutic agent that solely targets tumor cells bearing mutant *p110*α
349 without the systemic adverse effects of inhibiting WT signaling.

350 With respect to the clinical relevance of our findings, a first-in-human, open-label, Phase
351 I/IB dose escalation study of oral daily GDC-0077 alone and in combination with endocrine and
352 targeted therapies for *PIK3CA*-mutant solid tumors is ongoing. The single-agent portion of the
353 study showed that GDC-0077 had a manageable safety profile with a maximum tolerated dose of
354 9 mg once daily (supported by a linear pharmacokinetic profile), with promising anti-tumor
355 activity (Juric et al., 2019). When combined at this dose with letrozole with and without palbociclib
356 (Jhaveri et al., 2019), or when combined with fulvestrant the safety profile was also manageable
357 with promising anti-tumor activity (Kalinsky et al., 2020). No drug-drug interactions were
358 observed in the letrozole ± palbociclib portion of the study (Jhaveri et al., 2019). Phase III trials
359 are now ongoing to assess efficacy and safety in a randomized, controlled manner in locally
360 advanced or metastatic HR-positive/HER2-negative breast cancer in combination with palbociclib
361 and fulvestrant (NCT04191499). To further leverage the degradation potential of GDC-0077 in
362 HER2-positive breast cancers, this work has also provided the rationale for a first-in-human, open-
363 label, Phase I/IB dose escalation study of oral daily GDC-0077 in combination with standards of
364 care (trastuzumab and pertuzumab) is also being enabled.

365

366 **Methods**

367 **Chemical reagents**

368 The proteasome inhibitor MG132 (474790) was obtained from Calbiochem EMD Millipore
369 (Billerica, MA). Chloroquine (14774) was obtained from Cell Signaling (Danvers, MA).
370 Ammonium Chloride NH4Cl (254134) was obtained from Sigma-Aldrich (St. Louis, MO). PI3K
371 inhibitors and ubiquitin-activating E1 inhibitor (Chen et al., 2011) were provided by the chemistry
372 department at Genentech, Inc. (South San Francisco, CA).

373

374 **Antibody reagents**

375 Antibodies to p110α (4249), cleaved poly (ADP-ribose) polymerase (PARP) (9541),
376 phosphorylated (phospho)-Akt Ser473 (4060), pS6 S235/236 (2111), anti-ubiquitin (3936), p110δ
377 (34050), HER3 (12708), HER2 (2242), pHER2 Y1221/Y1222 (2243), and pHER3 Y128 (4791)
378 were obtained from Cell Signaling (Danvers, MA). The antibody to β-actin (A5441) was from
379 Sigma-Aldrich. Antibodies to Ras (ab52939), p85α (ab133595), and p85β (ab28356) were
380 obtained from Abcam (Cambridge, MA). Ubiquitin reagent TUBE1 (UM101) was obtained from
381 LifeSensors, Inc. (Malvern, PA). The p55γ antibody (MAB6638) was obtained from R&D
382 Systems (Minneapolis MN). Antibodies to GAPDH (MAB374) and p110β (04-400) were obtained
383 from EMD Millipore.

384

385 **pPRAS40 ELISA assay**

386 SW48 isogenic cells were plated in 384-well tissue-culture treated assay plates (Cat. No. 781091;
387 Greiner Bio-One; Monroe, NC) and incubated overnight at 37°C and 5% CO_2. The three isogenic
388 SW48 lines (WT, E545K, and H1047R) were plated and assayed in parallel. The following day,
389 test compounds were serially diluted in DMSO and added to cells (final DMSO concentration of

390 0.5%). Cells were then incubated with drugs for 24 hours at 37°C and 5% CO_2. After 24 hours,
391 cells were lysed and phosphorylated proline-rich AKT substrate of 40 kDa (pPRAS40) levels were
392 measured using the Meso Scale Discovery (MSD®) custom pPRAS40 384w Assay Kit (Cat. No.
393 L21CA-1; Rockville, MD). Cell lysates were added to assay plates pre-coated with antibodies
394 against pPRAS40 and allowed to bind to the capture antibodies overnight at 4°C. The detection
395 antibody (anti-total pPRAS40, labeled with an electrochemiluminescent SULFO-TAG™) was
396 added to the bound lysate and incubated for 1 hour at room temperature. The MSD® Read Buffer
397 was added such that when voltage was applied to the plate electrodes, the labels bound to the
398 electrode surface emitted light. The MSD® Sector Instrument measured the intensity of the light
399 and quantitatively measured the amount of pPRAS40 in the sample. Percent inhibition of
400 pPRAS40 per concentration of compounds was calculated relative to untreated controls. The EC_{50}
401 values were calculated using the 4-parameter logistic nonlinear regression dose-response model.
402 Reported EC_{50} values indicate an average value from three independent experiments. Standard
403 deviations are reported as ± the reported EC_{50} values for each cell line. The EC_{50} in WT cells was
404 divided by EC_{50} in mutants to derive the fold-increase in potency in mutant cells.
405

406 **Viability assay CellTiter-Glo®**

407 Cells were seeded (1000–2000 cells/well) in 384-well plates for 16 hours. On day two, nine serial
408 1:3 compound dilutions were made in DMSO in a 96-well plate. The compounds were then further
409 diluted into growth media using a Rapidplate robot (Zymark Corp., Hopkinton, MA). The diluted
410 compounds were then added to quadruplicate wells in the 384-well cell plate and incubated at 37°C
411 and 5% CO_2. After 4 days, relative numbers of viable cells were measured by luminescence using
412 CellTiter-Glo® (Promega) according to the manufacturer's instructions and read on a Wallac

413 Multilabel Reader (PerkinElmer, Foster City). The EC^{50} calculations were carried out using Prism
414 6.0 software (GraphPad, San Diego). The GR calculations and figures were performed using R
415 scripts based on Hafner et al. (Hafner et al., 2016).
416
417 **Nucleosome ELISA**
418 MDA-MB-453, HCC202, and Cal85-1 cells were plated in 96-well tissue-culture treated assay
419 plates (Corning; Cat. No. 3904; Corning, NY) and incubated overnight at 37°C and 5% CO_2. The
420 following day, PI3K inhibitors were serially diluted in DMSO and added to cells (final DMSO
421 concentration of 0.5%). Cells were then incubated with drugs for 72 hours at 37°C and 5% CO_2.
422 After 72 hours, cells were lysed and centrifuged at 200 g for 10 min. Histone-associated DNA-
423 fragment levels were analyzed using the Cell Death Detection ELISAPLUS (Roche; Cat. No.
424 11920685001; Basel Switzerland). 20 μL of supernatant was added to each well of the streptavidin
425 capture plate followed by 80 μl of anti-histone-biotin, and DNA-peroxidase immunoreagent.
426 Plates were incubated at room temperature for 2 hours shaking (300 RPM). Contents of the plate
427 were removed followed by three washes with Incubation buffer. 100 μL of ABTS solutions was
428 added to each well and plates were incubated for 10–20 min, after which 100 μL of ABTS Stop
429 Solution was added to each well. Absorbance was measured at 405 nm and 490 nm of each plate.
430 Fold increases were generated by assessing the increased of absorbance (A405 nm–A490 nm) of
431 wells from cells treated with compounds, normalized to those treated with DMSO alone.
432
433 **Cell lines and cell culture**
434 Cell lines were obtained from the ATCC. All cell lines underwent authentication by Short Tandem
435 Repeat profiling, SNP fingerprinting, and mycoplasma testing (Yu et al., 2015). The isogenic colon

436 cancer cell lines SW48 human PIK3CA (H1047R/+) (HD103-005) and SW48 human PIK3CA
437 (E545K/+) (HD103-001) and SW48 parental line were obtained from Horizon Discovery Ltd.
438 (Cambridge, UK). Cell lines were grown under standard tissue-culture conditions in RPMI media
439 with 10% fetal bovine serum (Gibco, 10082-147), 100 U/mL penicillin- streptomycin (Gibco,
440 15140-122), 2 mmol/L L-glutamine (Gibco, 15030-081). *PIK3CA* mutation status and frequencies
441 of all cell lines are summarized in Figure 5B. Cells were treated with compounds for the indicated
442 periods of time. For rescue experiments, 1 μM final concentration of proteasome inhibitor MG132
443 (EMD Millipore; Cat. No. 474790-5MG; Darmstadt, Germany), 2 μM HER2 inhibitor lapatinib
444 (Selleckchem; Cat. No. GW-572016), or 2 μM Ubiquitin activating enzyme E1 inhibitor
445 (synthesized at Genentech), were added before cell harvest.
446

447 **CRISPR engineering of HCC1954 cells**

448 HCC1954 breast cancer cells were engineered using CRISPR to knock out either the *PIK3CA* WT
449 allele or the mutant alleles, to create an isogenic pair of cell lines designated as HCC1954_mutant
450 and HCC1954_WT. gRNAs were designed using the CRISPRtool (http://crispr.mit.edu) to
451 minimize potential off-target effects and cloned into pCas-Guide-EF1a-GFP vector (Blueheron
452 Biotech). To generate the HCC1954_mutant line bearing p110α H1047R as homozygous mutant,
453 two CRISPR-Cas9 constructs were designed. One was designed to specifically target the wild type
454 allele in exon 21 (gRNA H1047R-2, ATGAATGATGCACATCATGG) and the second designed
455 to target the intron of both WT and mutant alleles (gRNA H1047R-7,
456 ACATTTGAGCAAAGACCTGA). To generate the HCC1954_WT line, two CRISPR-Cas9
457 constructs were designed with one gRNA targeting the mutant allele in exon 21 (H1047R-5,
458 ATGAATGATGCACGTCATGG) and the second gRNA targeting the intron of both WT and

459 mutant alleles (H1047R-8, TATTAAACTCCTGACATGCC). Plasmids for each targeting pair
460 were co-transfected using Turbofectin (Thermofisher). After 48 hours cells were put under
461 selection with 1 ug/mL puromycin. Puromycin resistant cells were further selected by collecting
462 GFP expressing cells by flow cytometry, and clones were expanded in standard cell culture
463 conditions to create stable lines. Targeting efficiency of the CRISPR-induced allelic knockouts
464 was assessed by PCR flanking the target sites (forward: TGCTGTGAAGGAAAATGGAA,
465 (reverse: TGCAGTGTGGAATCCAGAGTGAGC), and clones further validated with qRT-PCR
466 and DNA sequencing.
467

468 **siRNA transfection**

469 Transfection of siRNA was carried out using Lipofectamine RANiMAX reagent (Thermofisher),
470 72 hours in advance of drug treatment.
471

472 **Western blots**

473 Protein concentration was determined using the Pierce BCA Protein Assay Kit. For immunoblots,
474 equal protein amounts were loaded and then separated by electrophoresis through NuPAGE Novex
475 Bis-Tris 4–12% gradient gels (Invitrogen). Proteins were transferred onto Nitrocellulose
476 membranes using the iBlot system and protocol from InVitrogen (Carlsbad, CA).
477

478 **Subcellular fractionation**

479 Cells were washed once with phosphate-buffered saline, before scraping into 0.8 ml/dish
480 hypotonic lysis buffer (HLB: 25 mM Tris–HCl pH7.5, 10 mM NaCl, 1 mM EDTA, protease and
481 phosphatase inhibitors). The cells were lysed by 30 strokes in a Dounce homogenizer, subjected

482 to centrifugation at 1500 g (3000 RPM) for 5 min to pellet nuclei and unbroken cells, followed by
483 centrifugation of the supernatant at 100,000 g (44,000 RPM) in TLA55 rotor for 40 min. The
484 supernatant (800 μL) was collected (S100 fraction) and the pellet resuspended in 200ul HLB plus
485 1% NP40 (P100 fraction). The resuspended pellet was centrifuged 5 min in high speed in
486 microfuge and supernatant collected.
487

488 **Immunoprecipitation and pulldown**

489 Cells were lysed in 20 mM TrisHCL pH 7.5, 137 mM NaCl, 1 mM EDTA, 1% NP40, 10% glycerol
490 plus protease and phosphatase inhibitors. For p110α immunoprecipitation, lysates were incubated
491 with p110α antibody (Cell Signaling, 4249) overnight. 50 μL of proteinA agarose beads were
492 added to each sample and incubated additional 2 hours. For ubiquitinated protein pulldown
493 experiment, cells were lysed in lysis buffer containing 200 μg/mL TUBE1 (Lifesensors UM101).
494 Lysates were isolated and added 50 μL of glutathione agarose beads (Sigma, G4705). The samples
495 were incubated overnight and captured ubiquitinated protein was eluted in SDS reducing sample
496 buffer.
497

498 **RNA isolation and *PIK3CA* allele-specific quantitative RT-PCR**

499 Total RNA was isolated from cells using RNeasy Plus Mini Kit (Qiagen) following the protocol
500 described in the kit. First-strand cDNA synthesis and RT-qPCR was carried out using One step
501 RT QPCR reagent (Roche). Resulting signal was detected on Applied Biosystems Real Time PCR
502 System. Primers and allele specific probes were:
503 *PIK3CA* H1047R-forward: GGCTTTGGAGTATTTCATGAAACA
504 *PIK3CA* H1047R-reverse: GAAGATCCAATCCATTTTTGTTGTC

505 *PIK3CA* H1047R WT-probe: ATGATGCACATCATGGT

506 *PIK3CA* H1047R Mut-probe: TGATGCACGTCATGGT

507 *PIK3CA* E545K-forward: GCAATTTCTACACGAGATCCTCTCT

508 *PIK3CA* E545K-reverse: CATTTTAGCACTTACCTGTGACTCCAT

509 *PIK3CA* E545K WT-probe: TGAAATCACTGAGCAGGAG

510 *PIK3CA* E545K Mut-probe: TGAAATCACTAAGCAGGA

511

512 **Intracellular drug concentration**

513 Taselisib (1 μM in RPMI medium) was added to *PIK3CA*-mutant and -WT cancer cell lines in
514 triplicate and incubated under standard culture conditions (37°C, 5% CO_2) for 18 hours. Medium
515 containing taselisib was aspirated and cells were washed twice with 1 mL of ice-cold Hank's
516 balanced salt solution (HBSS). Cells were lysed by sonication for 1 min in HBSS followed by the
517 addition of an equal volume of acetonitrile containing analytical internal standard (propranolol,
518 100 nM). The supernatant was analyzed in positive mode on a SCIEX API-4000 LC/MS/MS
519 system with the transitions of 461/418 and 260/116 for taselisib and propranolol, respectively. The
520 LC separations were achieved using a LUNA C18 column (4 μm, 50 x 2.1 mm) from Phenomenex,
521 Inc. (Torrance, CA) and Agilent 1100 series pumps consisting of mobile phase A (water containing
522 0.1% formic acid) and mobile phase B (acetonitrile containing 0.1% formic acid). The flow rate
523 through the system was 1 mL/min. The initial condition was set at 5% B, which was ramped to
524 95% B over 40 sec. After allowing the system to hold at 95% B for 20 sec, the gradient was
525 changed back to the initial condition of 5% B and was allowed to equilibrate for 54 sec before the
526 next injection. A parallel replicate plate containing *PIK3CA*-mutant and -WT cancer cells was
527 reserved for the determination of protein concentrations. Cells were washed with HBSS buffer and

528 then lysed with 0.5 mL of ProteaPrep cell lysis solution (Protea Biosciences, Morgantown, WV).
529 After 30 min, the solution was neutralized with 0.5 mL HBSS buffer and 100 μL of the lysed cells
530 were used to determine the protein concentration by the standard Bradford protein assay (Thermo
531 Scientific, Rockford, IL), with bovine serum albumin as a standard.
532
533 **PI3K ADP-Glo assays for Ki measurement**
534 As described in WO 2017/001645 A1, the PI3K lipid kinase reaction was performed in the
535 presence of PIP2:3PS lipid substrate (Promega #V1792) and ATP. Following the termination of
536 the kinase reaction, turnover of ATP to ADP by the phosphorylation of the lipid substrate was
537 detected using the Promega ADP-Glo™ (Promega #V1792) assay. Reactions were carried out
538 using the following conditions for each PI3K isoform: PI3Kalpha (Millipore #14-602-K) kinase
539 concentration 0.2 nM, ATP 40 μM, PIP2:3PS 50 μM; PI3Kbeta (Promega #V1751) kinase
540 concentration 0.6 nM, ATP 40 μM, PIP2:3PS 50 μM; PI3K delta (Millipore #14-604-K), kinase
541 concentration 0.25 nM, ATP 40 μM, PIP2:3PS 50 μM; PI3K gamma (Millipore #14-558-K),
542 kinase concentration 0.4 nM, ATP 25 μM, PIP2:3PS 50 μM. After 120 min of reaction time, the
543 kinase reaction was terminated. After the reaction, any ATP remaining was depleted leaving only
544 ADP. Then the Kinase Detection Reagent was added to convert ADP to ATP, which was used in
545 a coupled luciferin/luciferase reaction. The luminescent output was measured and was correlated
546 with kinase activity. All reactions were carried out at room temperature. For each PI3K isoform a
547 3 μL mixture (1:1) of enzyme/lipid substrate solution was added to a 384 well white assay plate
548 (Perkin Elmer #6007299) containing 50 μL of test compound or DMSO only for untreated
549 controls. The reaction was started by the addition of 2 μL ATP/$MgCl_2$. The kinase reaction buffer
550 contained 50 mM HEPES, 50 mM $NaCl_2$, 3 mM $MgCl_2$, 0.01% BSA, 1% DMSO, and enzyme and

551 substrate concentrations. The reaction was stopped by the addition of 10 μL ADP-Glo reagent.
552 Plates were read in a Perkin Elmer Envision system using luminescence mode. A 10-point dose
553 response curve was generated for each test compound. Ki values for each compound were
554 determined using the Morrison Equation.
555
556 **Kinetic solubility**
557 Compounds were dissolved in DMSO to a concentration of 10 mM. These solutions were diluted
558 into PBS buffer (pH 7.2, composed with NaCl, KCl, Na_2HPO_4, and KH_2PO_4) to a final compound
559 concentration of 100 μM, DMSO concentration of 2%, at pH 7.4. The samples were shaken for 24
560 hours at room temperature followed by filtration. LC/CLND was used to determine compound
561 concentration in the filtrate, with the concentration calculated by a caffeine calibration curve and
562 the samples nitrogen content. An internal standard compound was spiked into each sample for
563 accurate quantification.
564
565 **Plasma protein binding**
566 As described in literature (Heffron et al., 2016), the extent of protein binding was determined in
567 vitro, in CD-1 mouse, Sprague–Dawley rat, and human plasma (Bioreclamation, Inc., Hicksville,
568 NY) by equilibrium dialysis using the RED Device (Thermo Fisher Scientific, Rockford, IL).
569 Compounds were added to pooled plasma ($n \geq 3$) at a total concentration of 5 μM. Plasma samples
570 were equilibrated with phosphate-buffered saline (pH 7.4) at 37°C in 90% humidity and 5% CO_2
571 for 4 hours. Following dialysis, compound concentration in plasma and buffer were measured by
572 LCMS/MS. The percent of unbound compound in plasma was determined by dividing the

573 concentration measured in the post-dialysis buffer by that measured in the post-dialysis plasma
574 and multiplying by 100.
575
576 **MDCK permeability**
577 Experiments were carried out as previously described (Irvine et al., 1999).
578
579 **Drug half-life *in vivo***
580 Experiments to determine half-life in mice were carried out as previously described (Furet et al.,
581 2013; Pang et al., 2014; Salphati et al., 2011).
582
583 **Pulse-chase**
584 Cells were starved in methionine/cysteine deficient media overnight. Cells were pulse labeled with
585 35S cysteine and methionine (Pro-mix l-[35S], Amersham) in RPMI lacking cysteine and
586 methionine for 6 hours, followed by three washes with RPMI containing no label. Cells were then
587 incubated in normal media containing methionine and cysteine, either with or without compounds.
588 Lysates were collected at various time points up to 48 hours. Radiolabeled p110α was
589 immunoprecipitated and run on SDS-PAGE. Images were acquired on the Typhoon Scanner (GE
590 Healthcare-Amersham), and signals quantified and normalized using ImageQuant TL software.
591 Data was fit to a single exponential decay function using Prism (GraphPad, San Diego, CA) with
592 Y=(Y0-NS)*exp(-K*X) + NS and constraints Y0=100, NS=0.
593
594 **Animal studies**

595 The in vivo efficacy of PI3K inhibitors was tested in three breast cancer xenograft models that
596 harbor *PIK3CA* mutations, HCC1954 (HER2-positive, *PIK3CA* H1047R), WHIM20 (ER-
597 positive/HER2-negative, *PIK3CA* H1047R) and HCI-003 (ER-positive/HER2-negative, *PIK3CA*
598 E545K). All in vivo studies were approved by Genentech and Institutional Animal Care and Use
599 Committee (IACUC) and adhered to the NIH Guidelines for the Care and Use of Laboratory
600 Animals. HCC1954 tumor cells (5x106) were inoculated in the 2/3 mammary fat pads of female
601 NCR nude mice (Taconic Farms, Hudson NY) while WHIM20 and HCI-003 tumors (50mm^3) were
602 engrafted in 2/3 mammary fat pads in female NOD-SCID gamma mice (Jackson Laboratories, Bar
603 Harbor, Maine). Tumor volumes were measured using Ultra Cal-IV calipers (Model 54-10-111;
604 Fred V.Fowler Co.; Newton, MA). The following formula was used in Excel, version 11.2 to
605 calculate tumor volume: Tumor Volume (mm^3) = (Length x Width^2) x 0.5. Mice for efficacy
606 studies were distributed into 8–10 mice/group with a mean tumor volume of 200 to 250 mm^3 at
607 the initiation of dosing. A linear mixed effect (LME) modeling approach was used to analyze the
608 repeated measurement of tumor volumes from the same animals over time (Pinheiro et al., 2017).
609 Cubic regression splines were used to fit a non-linear profile to the time courses of log^2 tumor
610 volume at each dose level. These non-linear profiles were then related to dose within the mixed
611 model. Tumor growth inhibition as a percentage of vehicle control (%TGI) was calculated as the
612 percentage of the area under the fitted curve (AUC) for the respective dose group per day in
613 relation to the vehicle, using the following formula: %TGI=100 x (1 - AUCdose/AUCvehicle).
614 The PI3K inhibitors taselisib, GDC-0941, GDC-0077, and BYL719 were formulated in
615 Methylcellulose Tween (MCT) vehicle consisting of 0.5% (w/v) methylcellulose, 0.2% (w/v)
616 polysorbate 80 (Tween-80) and dosed orally by gavage daily. Tumor sizes and mouse body
617 weights were recorded twice weekly, and mice with tumor volume exceeding 2000 mm^3 or body

618 weight loss of 20% of starting weight were promptly euthanized. For pharmacodynamic (PD) and
619 mechanistic studies, mice were dosed once by oral gavage and tumors harvested at 4 hours post-
620 dose. Following drug treatment, tumors were harvested and snap-frozen in liquid nitrogen,
621 dissociated in lysis buffer containing 10 μM Tris pH 7.4, 100 μM NaCl, 1 μM EDTA, 1 μM
622 EGTA, 1 μM NaF, 20 μM $Na_4P_2O_7$, 2 mM Na_3VO_4, 1% Triton X-100, 10% glycerol, 0.1% SDS,
623 and 0.5% deoxycholate supplemented with a phosphatase and protease inhibitor cocktail (Sigma,
624 St. Louis, MO). Protein concentrations were determined in whole cell lysates using the BCA
625 Protein Assay Kit (Pierce; Rockford, IL). Membrane fractions were isolated from xenograft tumors
626 as described above, and assessed by western blot.
627
628 **Mass spectrometry**
629 Liquid chromatography-tandem mass spectrometry (LC-MS/MS) analysis was performed on
630 p110α protein immunoprecipitated from three cell lines: HCC1954, HCC202 and HDQ-P1. Each
631 cell line was treated for 24 hours with either DMSO (vehicle) or taselisib (500 nM). Each
632 experiment was performed beginning with 4–6 mg protein lysate per cell line/treatment (total of 6
633 samples/experiment) for n=4 biological replicates. One gel region per sample, corresponding to
634 the expected migration was excised based on the migration of purified p110α protein in an adjacent
635 lane. Gel pieces were diced into ~1 mm^3 pieces and subjected to in-gel digestion as follows. Gel
636 pieces were de-stained with 50 mM ammonium bicarbonate/50% acetonitrile and dehydrated with
637 100% acetonitrile prior to reduction and alkylation using 50 mM dithiothreitol (30 min, 50°C) and
638 50 mM iodoacetamide (20 min, room temperature), respectively. Gel pieces were again
639 dehydrated, allowed to reswell in a 20 ng/μL trypsin in 50 mM ammonium bicarbonate/5%
640 acetonitrile digestion buffer on ice for 2 hours, and then transferred to a 37°C oven for overnight

641 incubation. Digested peptides were transferred to microcentrifuge tubes and gel pieces were
642 extracted twice, once with 50% acetonitrile/0.5% trifluoroacetic acid, and a second round with
643 100% acetonitrile. Extracts were combined with digested peptides and speed-vac dried to
644 completion. Samples were reconstituted in 5% formic acid/0.1% heptafluorobutyric acid/0.01%
645 hydrogen peroxide 30 min prior to LC-MS/MS analysis. Samples were analyzed by LC-MS/MS
646 with duplicate injection (with the exception of the first replicate where samples were injected once)
647 on a Thermo LTQ Orbitrap Elite coupled to a Waters nanoAcquity UPLC. Peptides were loaded
648 onto a 0.1mm X 100mm Waters Symmetry C18 column packed with 1.7 μm BEH-130 resin and
649 separated via a two-stage linear gradient where solvent B (98% acetonitrile, 2% water) was ramped
650 from 5% to 25% over 20 min and then from 25% to 50% over 2 min. Data were acquired in data
651 dependent mode with Orbitrap full MS scans collected at 60,000 resolution and the top 15 most
652 intense precursors selected for CID MS/MS fragmentation in the ion trap. MS2 spectra were
653 searched using Mascot, both against a concatenated target-decoy Uniprot database of human
654 proteins as well as against a small database containing wild-type, E545K and H1047R mutant
655 p110α sequences in order to identify mutant peptides. Peptide spectral matches for the Uniprot
656 search were rough filtered using linear discriminant analysis to 10% false discovery rate, then
657 confirmed via manual inspection. Extracted ion chromatograms and peak area integration for
658 p110α peptides were generated with 10 ppm mass tolerances using in-house software (MSPlorer).
659 Peak area data for each of 14 peptides (see Figure 3D and Figures S4C and S4D) were normalized
660 on a per-replicate basis to the most abundant peak area among the six samples. In cases where
661 duplicate injections (technical replicates) were available, normalized data for the two replicates
662 were averaged to generate a single normalized peak area per peptide-condition-experiment for the
663 protein sequence plots (Figure S4C). For statistical analysis, unnormalized peak areas across the

664 four biological replicates were consolidated in R using linear mixed effects modelling (lme4
665 package) to determine the relative ratio and measures of uncertainty (from which can be derived
666 p-values, confidence intervals, etc) for the comparison of DMSO (vehicle) versus taselisib (500
667 nM) treatments per cell line for each of total p110α, WT p110α, and mutant p110α (Bates et al.,
668 2015). Total p110α was determined based on the data generated from the following peptides:
669 EATLITIK (residues 39-46; 444.77481 m/z), DLNSPHSR (155-162; 463.22945 m/z),
670 LCVLEYQGK (241-249), VCGCDEYFLEK (254-264; 710.30246 m/z), VPCSNPR (376-382),
671 EAGFSYSHAGLSNR (503-516; 748.35281 m/z), YEQYLDNLLVR (641-651; 713.37540 m/z),
672 FGLLLESYCR (684-693; 629.32042 m/z), and LINLTDILK (712-720; 521.83039 m/z). For cells
673 bearing the H1047R mutation (i.e. HCC-1954), WT p110α was determined based on the
674 QMNDAHHGGWTTK (1042-1054; 749.82824 m/z) peptide and mutant p110α based on
675 QMNDAR (1042-1047; 375.66360 m/z) and HGGWTTK (1048-1054; 393.6983 m/z) peptides.
676 For cells bearing the E545K mutation (i.e. HCC-202), WT p110α was determined based on the
677 DPLSEITEQEK (538-548; 644.81917 m/z) peptide and mutant p110α based on DPLSEITK (538-
678 545; 451.74627 m/z) peptides. Peptides from these two mutant loci were not considered when
679 determining total p110α. Whenever applicable, cysteine residues within p110α peptides were
680 analysed in their carbamidomethylated form (+57.0215 Da) and methionine residues quantified
681 based on their singly oxidized (Met630 sulfoxide) form (+15.9949 Da). Quantified peptide peak
682 areas observed after treatment with taselisib or DMSO were analysed to estimate differential
683 abundances and accompanying measures of uncertainty for total, WT, and mutant, respectively,
684 across the two treatments. These three fractional abundances were combined to estimate the
685 relative proportions (and associated 95% confidence intervals) of WT versus mutant in each
686 mutant-containing cell line in both the DMSO and taselisib treated conditions by applying the

687 conservation of mass principle, as follows. Suppose "p" and "1-p" denote the fractions of WT and
688 mutant p110α, respectively, in a DMSO-treated cell culture. Comparing peptides quantified after
689 treatment with taselisib or DMSO from the total, WT-only, and mutant-only categories detailed
690 above, define the three fractions: f_total = fraction of total p110α remaining after taselisib, relative
691 to DMSO f_WT = fraction of WT p110alpha remaining after taselisib, relative to DMSO f_mut =
692 fraction of mutant p110α remaining after taselisib, relative to DMSO. The conservation of mass
693 principle requires that f_total = f_WT * p + f_mut * (1-p). Solving for "p" (the fraction of WT
694 p110α in DMSO-treated cells) yields an estimate of p = (f_total – f_mutant) / (f_WT - f_mutant
695) where log-scale estimates of the three fractions {f_total, f_WT, f_mutant} are obtained from the
696 linear mixed effects model. All other quantities of interest (with estimated standard errors,
697 confidence intervals, p-values, etc.) likewise can be estimated as functions of these three fractions
698 and their measures of uncertainty, which are also obtained from the linear mixed effects model.
699 Data are plotted as relative intensity values normalized to 1.0 and error bars represent the 95%
700 confidence intervals for each measurement based on the linear effects model.
701
702 **Declaration of interests:** All Genentech authors are employees and shareholders at Roche.
703
704 **Acknowledgements**
705 Support for third-party editing assistance for this manuscript, furnished by Daniel Clyde, PhD, of
706 Health Interactions, was provided by F. Hoffmann-La Roche Ltd.
707
708 **References**
709 Backer, J.M. (2010). The regulation of class IA PI 3-kinases by inter-subunit interactions. Curr
710 Top Microbiol Immunol *346*, 87-114.

711 Bates, D., Mächler, M., Bolker, B., and Walker, S. (2015). Fitting Linear Mixed-Effects Models
712 Using lme4. Journal os Statistical Software *67*, 48.
713 Burke, J.E., Perisic, O., Masson, G.R., Vadas, O., and Williams, R.L. (2012). Oncogenic mutations
714 mimic and enhance dynamic events in the natural activation of phosphoinositide 3-kinase
715 p110alpha (PIK3CA). Proc Natl Acad Sci U S A *109*, 15259-15264.
716 Burke, J.E., and Williams, R.L. (2013). Dynamic steps in receptor tyrosine kinase mediated
717 activation of class IA phosphoinositide 3-kinases (PI3K) captured by H/D exchange (HDX-MS).
718 Adv Biol Regul *53*, 97-110.
719 Cantley, L.C., Auger, K.R., Carpenter, C., Duckworth, B., Graziani, A., Kapeller, R., and Soltoff,
720 S. (1991). Oncogenes and signal transduction. Cell *64*, 281-302.
721 Chen, J.J., Tsu, C.A., Gavin, J.M., Milhollen, M.A., Bruzzese, F.J., Mallender, W.D., Sintchak,
722 M.D., Bump, N.J., Yang, X., Ma, J., *et al*. (2011). Mechanistic studies of substrate-assisted
723 inhibition of ubiquitin-activating enzyme by adenosine sulfamate analogues. J Biol Chem *286*,
724 40867-40877.
725 Cheng, H., Liu, P., Ohlson, C., Xu, E., Symonds, L., Isabella, A., Muller, W.J., Lin, N.U., Krop,
726 I.E., Roberts, T.M., *et al*. (2016). PIK3CA(H1047R)- and Her2-initiated mammary tumors escape
727 PI3K dependency by compensatory activation of MEK-ERK signaling. Oncogene *35*, 2961-2970.
728 Echeverria, I., Liu, Y., Gabelli, S.B., and Amzel, L.M. (2015). Oncogenic mutations weaken the
729 interactions that stabilize the p110alpha-p85alpha heterodimer in phosphatidylinositol 3-kinase
730 alpha. FEBS J *282*, 3528-3542.
731 Engelman, J.A., Chen, L., Tan, X., Crosby, K., Guimaraes, A.R., Upadhyay, R., Maira, M.,
732 McNamara, K., Perera, S.A., Song, Y., *et al*. (2008). Effective use of PI3K and MEK inhibitors to
733 treat mutant Kras G12D and PIK3CA H1047R murine lung cancers. Nat Med *14*, 1351-1356.
734 Folkes, A.J., Ahmadi, K., Alderton, W.K., Alix, S., Baker, S.J., Box, G., Chuckowree, I.S., Clarke,
735 P.A., Depledge, P., Eccles, S.A., *et al*. (2008). The identification of 2-(1H-indazol-4-yl)-6-(4-
736 methanesulfonyl-piperazin-1-ylmethyl)-4-morpholin-4-yl-t hieno[3,2-d]pyrimidine (GDC-0941)
737 as a potent, selective, orally bioavailable inhibitor of class I PI3 kinase for the treatment of cancer.
738 J Med Chem *51*, 5522-5532.
739 Furet, P., Guagnano, V., Fairhurst, R.A., Imbach-Weese, P., Bruce, I., Knapp, M., Fritsch, C.,
740 Blasco, F., Blanz, J., Aichholz, R., *et al*. (2013). Discovery of NVP-BYL719 a potent and selective

741 phosphatidylinositol-3 kinase alpha inhibitor selected for clinical evaluation. Bioorg Med Chem
742 Lett *23*, 3741-3748.
743 Greig, M.J., Niessen, S., Weinrich, S.L., Feng, J.L., Shi, M., and Johnson, T.O. (2015). Effects of
744 Activating Mutations on EGFR Cellular Protein Turnover and Amino Acid Recycling Determined
745 Using SILAC Mass Spectrometry. Int J Cell Biol *2015*, 798936.
746 Hafner, M., Niepel, M., Chung, M., and Sorger, P.K. (2016). Growth rate inhibition metrics correct
747 for confounders in measuring sensitivity to cancer drugs. Nat Methods *13*, 521-527.
748 Heffron, T.P., Heald, R.A., Ndubaku, C., Wei, B., Augistin, M., Do, S., Edgar, K., Eigenbrot, C.,
749 Friedman, L., Gancia, E., *et al*. (2016). The Rational Design of Selective Benzoxazepin Inhibitors
750 of the alpha-Isoform of Phosphoinositide 3-Kinase Culminating in the Identification of (S)-2-((2-
751 (1-Isopropyl-1H-1,2,4-triazol-5-yl)-5,6-dihydrobenzo[f]imidazo[1,2-d][1 ,4]oxazepin-9-
752 yl)oxy)propanamide (GDC-0326). J Med Chem *59*, 985-1002.
753 Irvine, J.D., Takahashi, L., Lockhart, K., Cheong, J., Tolan, J.W., Selick, H.E., and Grove, J.R.
754 (1999). MDCK (Madin-Darby canine kidney) cells: A tool for membrane permeability screening.
755 J Pharm Sci *88*, 28-33.
756 Isakoff, S.J., Engelman, J.A., Irie, H.Y., Luo, J., Brachmann, S.M., Pearline, R.V., Cantley, L.C.,
757 and Brugge, J.S. (2005). Breast cancer-associated PIK3CA mutations are oncogenic in mammary
758 epithelial cells. Cancer Res *65*, 10992-11000.
759 Jackson, S.P., Schoenwaelder, S.M., Goncalves, I., Nesbitt, W.S., Yap, C.L., Wright, C.E.,
760 Kenche, V., Anderson, K.E., Dopheide, S.M., Yuan, Y., *et al*. (2005). PI 3-kinase p110beta: a new
761 target for antithrombotic therapy. Nat Med *11*, 507-514.
762 Jhaveri, K., Kalinsky, K., Bedard, P.L., Cervantes, A., Saura, C., Krop, I.E., Hamilton, E., Schmid,
763 P., Varga, A., Turner, N., *et al*. (2019). Phase Ib dose escalation study evaluating the mutant
764 selective PI3K-alpha inhibitor GDC-0077 in combination with letrozole with and without
765 palbociclib in patients with PIK3CA-mutant HR+/HER2- breast cancer. In San Antonio Breast
766 Cancer Symposium (San Antonio).
767 Juric, D., Kalinsky, K., and Oliveira, M. (2019). A first-in-human phase Ia dose escalation study
768 of GDC-0077, a p110a-selective and mutant-degrading PI3K inhibitor, in patients with PIK3CA-
769 mutant solid tumors. In San Antonio Breast Cancer Symposium (San Antonio, TX, USA).
770 Juric, D., Krop, I., Ramanathan, R.K., Wilson, T.R., Ware, J.A., Sanabria Bohorquez, S.M.,
771 Savage, H.M., Sampath, D., Salphati, L., Lin, R.S., *et al*. (2017). Phase I Dose-Escalation Study

772 of Taselisib, an Oral PI3K Inhibitor, in Patients with Advanced Solid Tumors. Cancer Discov *7*,
773 704-715.
774 Kalinsky, K., Juric, D., Bedard, P.L., Oliveira, M., Cervantes, A., Hamilton, E., Krop, I.E., Turner,
775 N., Schmid, P., Varga, A., *et al*. (2020). A phase I/Ib study evaluating GDC-0077 plus fulvestrant
776 in patients with PIK3CA-mutant, hormone receptor-positive/HER2-negative breast cancer In
777 AACR Annual Meeting.
778 Kang, S., Bader, A.G., and Vogt, P.K. (2005). Phosphatidylinositol 3-kinase mutations identified
779 in human cancer are oncogenic. Proc Natl Acad Sci U S A *102*, 802-807.
780 Krop, I.E., Mayer, I.A., Ganju, V., Dickler, M., Johnston, S., Morales, S., Yardley, D.A., Melichar,
781 B., Forero-Torres, A., Lee, S.C., *et al*. (2016). Pictilisib for oestrogen receptor-positive, aromatase
782 inhibitor-resistant, advanced or metastatic breast cancer (FERGI): a randomised, double-blind,
783 placebo-controlled, phase 2 trial. Lancet Oncol *17*, 811-821.
784 Martin, M., Chan, A., Dirix, L., O'Shaughnessy, J., Hegg, R., Manikhas, A., Shtivelband, M.,
785 Krivorotko, P., Batista Lopez, N., Campone, M., *et al*. (2017). A randomized adaptive phase II/III
786 study of buparlisib, a pan-class I PI3K inhibitor, combined with paclitaxel for the treatment of
787 HER2- advanced breast cancer (BELLE-4). Ann Oncol *28*, 313-320.
788 Mayer, I.A., Abramson, V.G., Formisano, L., Balko, J.M., Estrada, M.V., Sanders, M.E., Juric,
789 D., Solit, D., Berger, M.F., Won, H.H., *et al*. (2017). A Phase Ib Study of Alpelisib (BYL719), a
790 PI3Kalpha-Specific Inhibitor, with Letrozole in ER+/HER2- Metastatic Breast Cancer. Clin
791 Cancer Res *23*, 26-34.
792 Miled, N., Yan, Y., Hon, W.C., Perisic, O., Zvelebil, M., Inbar, Y., Schneidman-Duhovny, D.,
793 Wolfson, H.J., Backer, J.M., and Williams, R.L. (2007). Mechanism of two classes of cancer
794 mutations in the phosphoinositide 3-kinase catalytic subunit. Science *317*, 239-242.
795 Pang, J., Baumgardner, M., Cheong, J., Edgar, K., Heffron, T.P., and Le, H. (2014). Preclinical
796 Evaluation of the β Isoform-sparing PI3K inhibitor GDC-0032 and prediction of its human
797 pharmacokinetics. Drug Metabolism Reviews *45*.
798 Pinheiro, J., Bates, D., DebRoy, S., Sarkar, D., and Team, t.R.C. (2017). Linear and Nonlinear
799 Mixed Effects Models. R package version 3.1-131.
800 Rodon, J., Dienstmann, R., Serra, V., and Tabernero, J. (2013). Development of PI3K inhibitors:
801 lessons learned from early clinical trials. Nat Rev Clin Oncol *10*, 143-153.

802 Sadhu, C., Masinovsky, B., Dick, K., Sowell, C.G., and Staunton, D.E. (2003). Essential role of
803 phosphoinositide 3-kinase delta in neutrophil directional movement. J Immunol *170*, 2647-2654.
804 Salphati, L., Pang, J., Plise, E.G., Chou, B., Halladay, J.S., Olivero, A.G., Rudewicz, P.J., Tian,
805 Q., Wong, S., and Zhang, X. (2011). Preclinical pharmacokinetics of the novel PI3K inhibitor
806 GDC-0941 and prediction of its pharmacokinetics and efficacy in human. Xenobiotica *41*, 1088-
807 1099.
808 Samuels, Y., Diaz, L.A., Jr., Schmidt-Kittler, O., Cummins, J.M., Delong, L., Cheong, I., Rago,
809 C., Huso, D.L., Lengauer, C., Kinzler, K.W., *et al*. (2005). Mutant PIK3CA promotes cell growth
810 and invasion of human cancer cells. Cancer Cell *7*, 561-573.
811 Yu, J., Zhang, Y., McIlroy, J., Rordorf-Nikolic, T., Orr, G.A., and Backer, J.M. (1998). Regulation
812 of the p85/p110 phosphatidylinositol 3'-kinase: stabilization and inhibition of the p110alpha
813 catalytic subunit by the p85 regulatory subunit. Mol Cell Biol *18*, 1379-1387.
814 Yu, M., Selvaraj, S.K., Liang-Chu, M.M., Aghajani, S., Busse, M., Yuan, J., Lee, G., Peale, F.,
815 Klijn, C., Bourgon, R., *et al*. (2015). A resource for cell line authentication, annotation and quality
816 control. Nature *520*, 307-311.
817

818 **Figure Legends**

819 **Figure 1**

820 **GDC-0032 and GDC-0077 have increased potency in *PIK3CA*-mutant cancer cells**

821 **(A)** Chemical structures and physicochemical properties of PI3K inhibitors.

822 [a]Inhibition of ATP-hydrolysis by PI3K isoforms in a biochemical assay, ADP production measured

823 by ADP-Glo™. [b]Plasma protein binding determined by equilibrium dialysis.

824 [c] Permeability measured using Madin-Darby canine kidney (MDCK) epithelial cells; A = apical,

825 B = basolateral. B→A / A→B used to estimate efflux potential.[d] Mouse PO dose as MCT

826 suspension.

827 **(B)** Cell viability IC_{50} values determined by quantifying ATP from all tumor lines at 5 days post-

828 treatment.

829 **(C)** PI3K inhibitor potency in SW48 isogenic *PIK3CA*-mutant and -wild-type parental cells in a

830 4-day viability assay. Error bars are standard deviation of quadruplicates

831 **(D)** *In vivo* efficacy of taselisib, GDC-0077, and BYL719 in HCC1954 PIK3CA H1047R breast

832 cancer xenograft model.

833

834 **Figure 2**

835 **Activity of PI3Kα inhibitors in combination with palbociclib in HR-positive breast cancer**

836 **cells**

837 **(A)** Dose response curve of MCF-7 cells treated with GDC-0077 either alone (blue), without E2

838 to mimic aromatase inhibitor (dark blue), with palbociclib at 0.15μM (purple), or with palbociclib

839 at 0.15 μM (purple) and without E2 (dark purple). Negative values indicate a cytotoxic response.

840 y-axis shows normalized growth inhibition (GR value).

841 **(B)** Growth response of 5 HR-positive breast cancer cells with *PIK3CA* mutations to treatment
842 with either palbociclib at 0.15 μM (red), E2 withdrawal (gray), GDC-0077 at 0.123 μM (blue),
843 Palbociclib at 0.15μM and E2 withdrawal (dark red), or the triple combination (dark purple). y-
844 axis shows normalized growth inhibition (GR value).
845 **(C)** Efficacy of palbociclib, fulvestrant and GDC-0077 as single agent or in combination in MCF7
846 xenografts. Each group contains 12 animals at the beginning of the experiment.
847
848 **Figure 3**
849 **Taselisib depletes mutant p110α protein through ubiquitin and proteasome mechanism in a**
850 **dose and time dependent manner**
851 **(A)** Western blots of the inhibitor response in PI3K signaling (pHER3 and pAKT) in *PIK3CA*-
852 mutant (HCC1954, HCC202, and MDA-MB-453) cell lines treated with 1 μM BYL719 or 0.5 μM
853 GDC-0077 for indicated time points.
854 **(B)** Mass spectrometry of HCC1954 cells treated for 24 hours with 500 nM taselisib. A neo-tryptic
855 peptide generated from PIK3CA H1047R was used to assess mutant protein levels compared to
856 wild-type protein in the same lysate.
857 **(C)** Rescue of taselisib- or GDC-0077-mediated p110α degradation in HCC1954 cells by either a
858 proteasome inhibitor (MG132) or a Ubiquitin Activating Enzyme E1 (UAE1) inhibitor.
859 **(D)** HCC1954 PIK3CA H1047R cells were treated 8 hours or HCC202 PIK3CA E545K cells were
860 treated for 18 hours with either DMSO or 1 μM taselisib ± MG132 or ± UAE1 inhibitor. Protein
861 lysates were run on western blot and probed with antibodies to p110α, pAKT, and b-actin, or
862 ubiquitinated proteins were pulled-down with TUBE1 reagent and then blotted with anti-p110α
863 antibody.

864 **(E)** HCC1954 cells engineered to be isogenic for *PIK3CA*-mutant or -wild-type were treated with
865 1 μM taselisib for up to 48 hrs followed by western blotting. Experimental replicates n=3 were
866 used to quantify p110α.
867 **(F)** Pulse-chase of isogenic cell lines, HCC1954_mutant and HCC1954_wild-type. PI3K inhibitor
868 taselisib at 1 μM was added during the chase. Pull-down with p110α antibody was followed by
869 autoradiography, and data fit to a single exponential decay function.
870
871 **Figure 4**
872 **Taselisib-mediated degradation of mutant p110αha occurs preferentially at the plasma**
873 **membrane**
874 **(A)** Subcellular fractionation of isogenic HCC1954_mutant and HCC1954_wild-type cells. Pull
875 down of ubiquitinated protein was followed by western blotting with anti-p110α.
876 **(B)** HCC1954_mutant cells were transfected with p85α, p85β or p55gγ isoform specific siRNA
877 followed by 1 μM taselisib treatment.
878 **(C)** HCC1954_mutant cell line was treated with 1 μM taselisib for up to 24 hours. Cell lysates
879 were precipitated with p85γ or p85β antibody, followed by immunoblot with antibodies indicated
880 to the left.
881 **(D)** HCC1954_mutant cells were transfected with p85α or p85β siRNA followed by taselisib
882 treatment. Cells were harvested at various time points and fractionated. K63 or K48 linked
883 ubiquitin conjugated protein was pulled down from membrane fraction and analyzed by
884 immunoblotting with p110α antibody.
885
886 **Figure 5**

887 **Taselisib- and GDC-0077-induced mutant p110α degradation is dependent on RTK activity**

888 **(A)** Cell viability IC_{50} values determined by quantifying ATP from breast tumor lines: HER2-
889 positive *PIK3CA*-mutant (n=6), HER2-positive *PIK3CA*-wild-type (n=4), HER2-negative
890 *PIK3CA*-mutant (n=10), and HER2-negative *PIK3CA*-wild-type (n=20) at 5 days post-treatment.

891 **(B)** Bar plot showing *PIK3CA*-mutant frequency among tumor lines harboring *PIK3CA* hotspot
892 mutations. ATP based cell viability assay in selected cell line (HCC2185, SW948, EFM-19,
893 HCC1954, T-47D, NCI-1048, VP303, MDAMB453 and KPL4). western blot of the p110α protein
894 levels and pAKT signaling in same cell lines treated with GDC-0077 for indicated concentrations
895 for 24 hours.

896 **(C)** HER2-negative *PIK3CA*-wild-type or -mutant cells cultured in standard media with 10% FBS
897 and treated with GDC-0077 alone or addition of growth factors (EGF and neuregulin).

898 **(D)** HCC1954 PIK3CA H1047R cells treated with taselisib alone or combination of taselisib and
899 lapatinib. Cell lysates were precipitated with p110α antibody, followed by western blot with HER3
900 antibody.

901 **(E)** Cell lysates following treatment with taselisib or GDC-0077 alone or combination with
902 lapatinib for indicated time points followed by western blot analysis with indicated antibodies.

903

904 **Figure 6:**

905 **p110α-mutant degrading inhibitors provide more benefit in HER2-positive versus HER2-**
906 **negative p110α-mutant cancers**

907 **(A)** Mechanistic model of drug-induced p110α degradation in HER2-positive and HER2-negative
908 *PIK3CA*-mutant cells.

909 **(B)** Tumor growth curve from KPL-4 (HER2+, PIK3CA H1047R) xenograft treated with vehicle,
910 taselisib, trastuzumab plus pertuzumab, or the indicated drug combination.
911 **(C)** Tumor growth curve from KPL-4 (HER2+, PIK3CA H1047R) xenograft treated with vehicle,
912 GDC-0077, TDM-1 or the indicated drug combination.
913
914 **Figure S1**
915 **Taselisib and GDC-0077 have increased potency in *PIK3CA*-mutant cancer cells**
916 **(A)** PI3K inhibitors assessed for apoptosis induction in mutant and wild-type breast cancer cell
917 lines in 72 hour Nucleosome ELISA. Error bars are standard deviation of triplicates.
918 **(B)** Cell potency in 4-day CellTiter-Glo® viability assay for taselisib and PI3Kα inhibitors
919 BYL719, GNE-102, GNE-326 in SW48 isogenic H1047R and wild-type cells. Error bars are
920 standard deviation of triplicates.
921 **(C)** Combination of PI3Kα inhibitor GNE-102 with PI3Kδ inhibitor idelalisib in 4-day viability
922 assay in HCC1954 PIK3CA H1047R mutant cells. Error bars are standard deviation of
923 quadruplicates.
924 **(D)** Combination of taselisib with PI3Kβ inhibitor TGX-221 in HCC1954 PIK3CA H1047R
925 mutant cells in a 4-day viability assay. Error bars are standard deviation of quadruplicates.
926 **(E)** Intracellular drug concentrations of taselisib in cancer cell lines treated for 18 hours with 1 μM
927 taselisib. Results of LC/MS/MS for triplicate wells are shown. Error bars are standard deviation
928 of triplicates.
929 **(F)** *In vivo* efficacy of GDC-0077 in PIK3CA H1047R breast cancer xenograft HCC1954 and
930 KPL4 models, and breast cancer HCI003 PDX (patient-derived xenograft) model. GDC-0077
931 dosed orally and daily (QD) in MCT (0.5 % methycellulose/0.2% Tween-80) vehicle.

932 **Figure S2:**

933 **Activity of GDC-0077 in combination with Palbociclib and/ or Fulvestrant**

934 **(A)** Dose response curve of MCF-7 cells treated with GDC-0077 alone (blue), without E2 to mimic

935 aromatase inhibitor (dark blue).

936 **(B)** Weight loss for MCF-7 xenograft experiment.

937 **(C)** Efficacy and weight loss for MDA-MB-453 xenograft experiment.

938

939 **Figure S3**

940 **Taselisib and GDC-0077 induce mutant p110α and not WT p110a degradation**

941 **(A)** Subcellular fractionation of HCC1954 PIK3CA H1047R mutant cells treated with PI3K

942 inhibitors taselisib or BYL719 for up to 8 hours, followed by p110α western blot.

943 **(B)** Taselisib and BYL719 treatment for 8 hours in HCC1954 PIK3CA H1047R mutant cells and

944 HDQ-P1 *PIK3CA*-wild-type cells.

945 **(C)** Quantitative RT-PCR shows no reduction in *PIK3CA* RNA expression in HCC1954 cells

946 treated with taselisib or BYL719 for up to 24 hours. Error bars are standard deviation of triplicates.

947 **(D)** Membrane-associated p110a expression following single oral dose of 15 mg/kg taselisib, 40

948 mg/kg BYL719, or 50 mg/kg GDC-0077 treatment in HCC1954 xenograft tumors.

949

950 **Figure S4**

951 **Taselisib depletes mutant p110α protein through ubiquitin and proteasome mechanism in a**

952 **dose and time dependent manner**

953

954 **(A)** *PIK3CA*-mutant cells were treated with PI3K inhibitors at concentrations relevant to plasma
955 concentrations achieved with clinically administered doses for pictilisib (GDC-0941) (330 mg),
956 taselisib (6 mg), and GDC-0077 (9 mg).
957 **(B)** Quantitative mass spectrometry analysis of p110α levels in HCC1954, HCC202 and HDQP1
958 cells treated with either DMSO or 500 nM taselisib for 24 hours (n=4). For each cell line, the
959 relative abundance of peptides from loci spanning the protein are compared between DMSO
960 (above line) and taselisib-treated (below line) cells. For mutant loci (H1047R in HCC1954 cells,
961 E545K in HCC202 cells), the protein sequence is split to depict the wild-type and mutant-specific
962 peptides in parallel.
963 **(C)** Mass spectrometry analysis of peptides representing wild-type and E545K mutant p110α from
964 HCC202 breast cancer cells treated for 24 hours with either DMSO or 500 nM taselisib. The neo-
965 trypic peptide generated from p110α E545K was used to assess mutant protein levels compared to
966 wild-type protein in the same lysate (n=4).
967 **(D)** Lysosomotropic agents chloroquine and ammonium chloride (NH_4Cl) do not rescue p110α
968 degradation induced by 1.6 μM taselisib in HCC1954 cells
969 **(E)** NGS and qRT-PCR for allele-specific mRNA expression in HCC1954 parental and isogenic
970 HCC1954_mutant and HCC1954_wild-type cells. Error bars are standard deviation of triplicates.
971 **(F)** HCC1954_mutant and HCC1954_wild-type isogenic cells were treated with 1.6 μM taselisib
972 for up to 9 hours. Pull down of ubiquitinated protein was followed by western blotting with anti-
973 p110α antibody.
974 **(G)** Subcellular fractionation of HCC1954_parental and isogenic HCC1954_mutant and
975 HCC1954_WT cells. Pull down of ubiquitinated protein was followed by western blotting with
976 anti-p110alpha .
977

978 **Figure S5**

979 **Taselisib-mediated degradation of mutant p110α occurs preferentially at the plasma**
980 **membrane.**

981 **(A)** HCC1954_mutant cells were treated with 1 μM taselisib alone or combination with
982 proteasome inhibitor MG132. Cell lysates were precipitated with p85α, p85β or p55γ antibody,
983 followed by immunoblot with antibodies indicated to the left. Real time qPCR assays of the p85
984 isoforms in RNA collected from untreated cells.

985 **(B)** HCC1954 cells were treated with 1.6 μM taselisib for 24 hours as indicated. Cell lysates were
986 prepared and total protein were applied to pRTK arrays. Arrows indicate RTKs whose
987 phosphorylation was up-regulated following the treatment.

988 **(C)** HCC1954_mutant cell line was treated with 1 μM taselisib alone or in combination with
989 proteasome inhibitor MG132. Cell lysates were precipitated with p85α, p85β or p55γ antibody,
990 followed by immunoblot with antibodies indicated to the left.

991 **(D)** HCC1954_mutant cell line was treated with 1 μM taselisib alone or in combination with
992 lapatinib. Cell lysates were precipitated with p85α or p85β antibody, followed by immunoblot
993 with antibodies indicated to the left.

994

995 **Figure S6**

996 **RTK activity plays a key role in regulating p110α degradation**

997 **(A)** Western blot for membrane associated p110α in a subset of treated (taselisib 20 mg/kg 4hr
998 single dose) versus untreated PDX tumors HCI-003, HCI-013, WHIM20, HCI-011, WHIM18.
999 Total lysates from untreated tumor were applied to pRTK arrays.

1000 **(B)** Cell lines were harvested after treatment with 0.5 μM GDC-0077 or 1 μM BYL719 at various
1001 time points followed by western blot analysis with indicated antibodies
1002 **(C)** Mechanistic model of drug-induced p110α degradation in heterozygous *PIK3CA*-mutant cells.
1003 SKBR3 (HER2-positive *PIK3CA*-wild-type) cells were treated with 0.5 μM GDC-0077 or 1 μM
1004 BYL719 at various time points followed by western blot analysis with indicated antibodies.
1005 **(D)** HCC1954 parental and *PIK3CA*-wild-type and -mutant isogenic cell lines are harvested after
1006 treatment with 0.5 μM GDC-0077 or 1 μM BYL719 at various time points followed by western
1007 blot analysis with indicated antibodies. Cell viability IC_{50} values determined by quantifying ATP
1008 from same cell lines at 5 days post-treatment.
1009 **(E)** HCC2911 parental and *PIK3CA*-wild-type and -mutant isogenic cell lines are harvested after
1010 treatment with 0.5 μM GDC-0077 or 1 μM BYL719 at various time points followed by western
1011 blot analysis with indicated antibodies. Cell viability IC_{50} values determined by quantifying ATP
1012 from same cell lines at 5 days posttreatment.
1013

Figure 1

A

	taselisib GDC-0032	GNE-326	GNE-102	pictilisib GDC-0941	alpelisib BYL719	GNE-181	GDC-0077
Structure							
p110a ATP K_i [a]	0.1 nM	0.3 nM	0.2 nM	2.6 nM	2.2 nM	0.4 nM	0.04 nM
Fold a vs. b / d / g [a]	591 / 0.9 / 16	502 / 22 / 102	1002 / 34 / 366	27 / 0.6 / 16	424 / 13 / 18	119 / 0.4 / 2	2676 / 337 / 574
Kinetic solubility	33 uM	107 uM	46 uM	37 uM	40 uM	2.1 uM	167 uM
Plasma protein binding [b] (%, H / R / M)	90 / 97 / 97	56 / 69 / 62	53 / 48 / 69	93 / 93 / 96	92 / 91 / 92	80 / 98 / 98	41 / 39 / 74
MDCK P_{app} AB/BA [c] (BA / AB)	6.4 x 10^{-6}cm/s (1.7)	8.5 x 10^{-6}cm/s (0.9)	2.2 x 10^{-6}cm/s (2.3)	7.6 x 10^{-6}cm/s (3.0)	11 x 10^{-6}cm/s (1.0)	11 x 10^{-6}cm/s (0.9)	1.9 x 10^{-6}cm/s (2.5)
Mouse $t_{1/2}$ AUC_{inf} dose [d]	2.1 hr 388 uM*hr 25 mg/kg	2.4 hr 74 uM*hr 25 mg/kg	2.6 hr 2 uM*hr 10 mg/kg	1.4 hr 11 uM*hr 25 mg/kg	3.1 hr 34 uM*hr 15 mg/kg	3.1 hr 291 uM*hr 25 mg/kg	4.3 hr 38 uM*hr 25 mg/kg

B

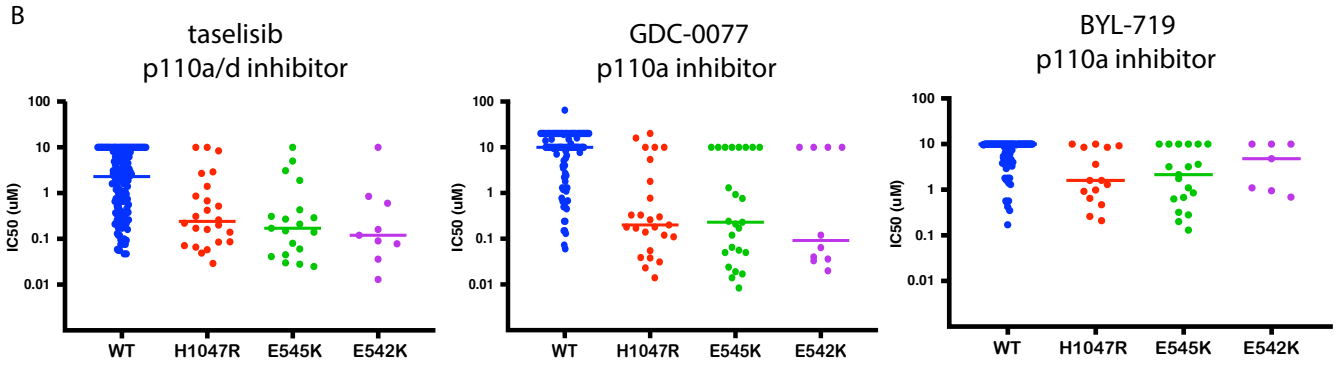

C

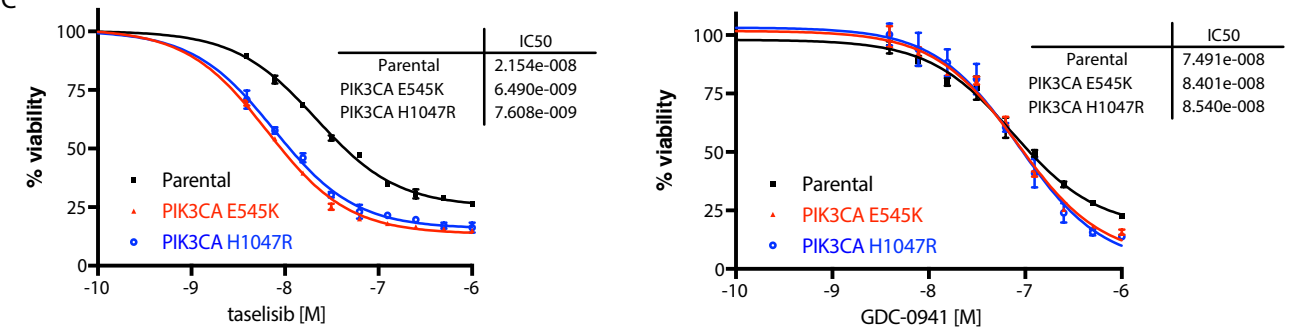

D

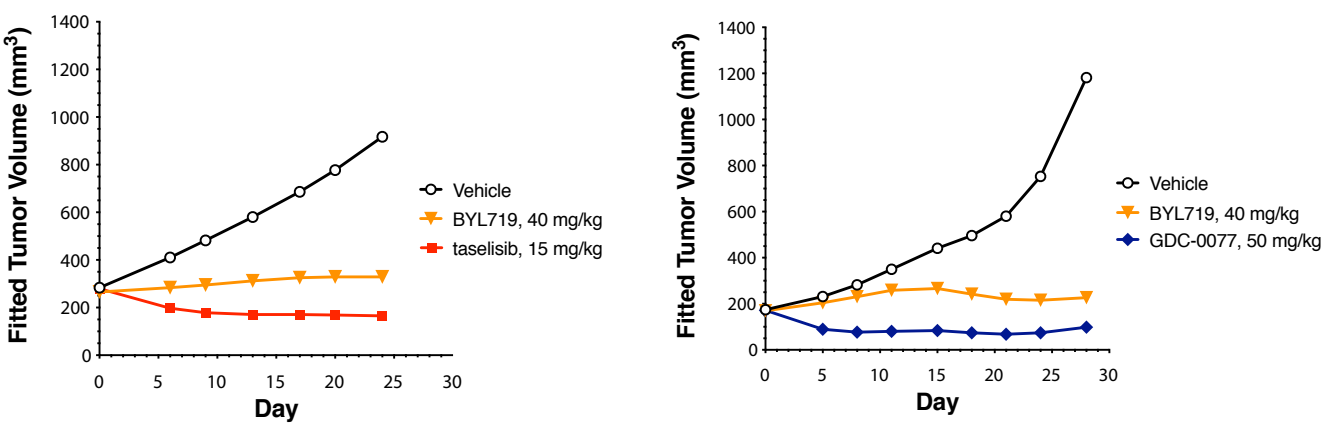

Figure 2

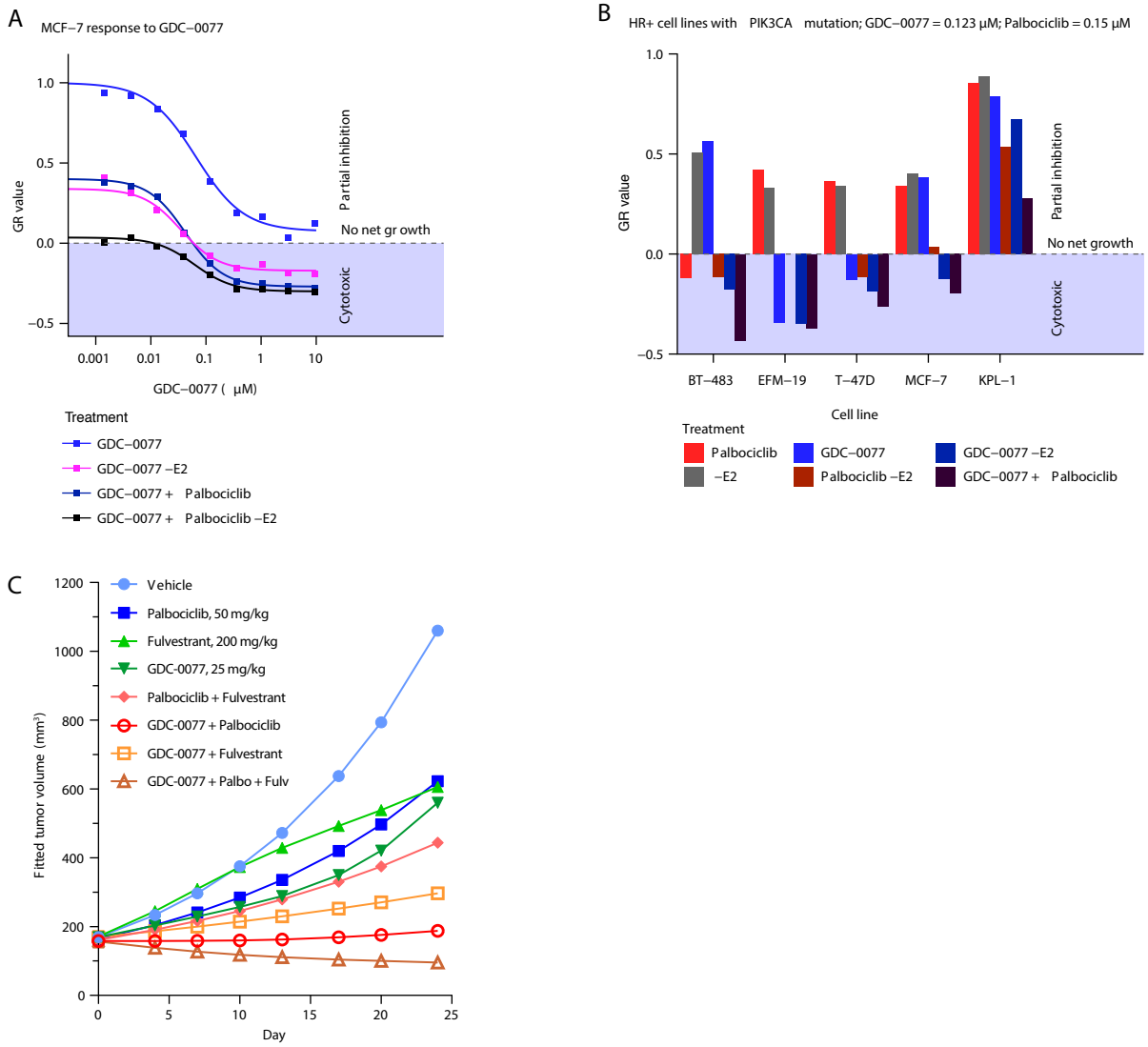

Figure 3

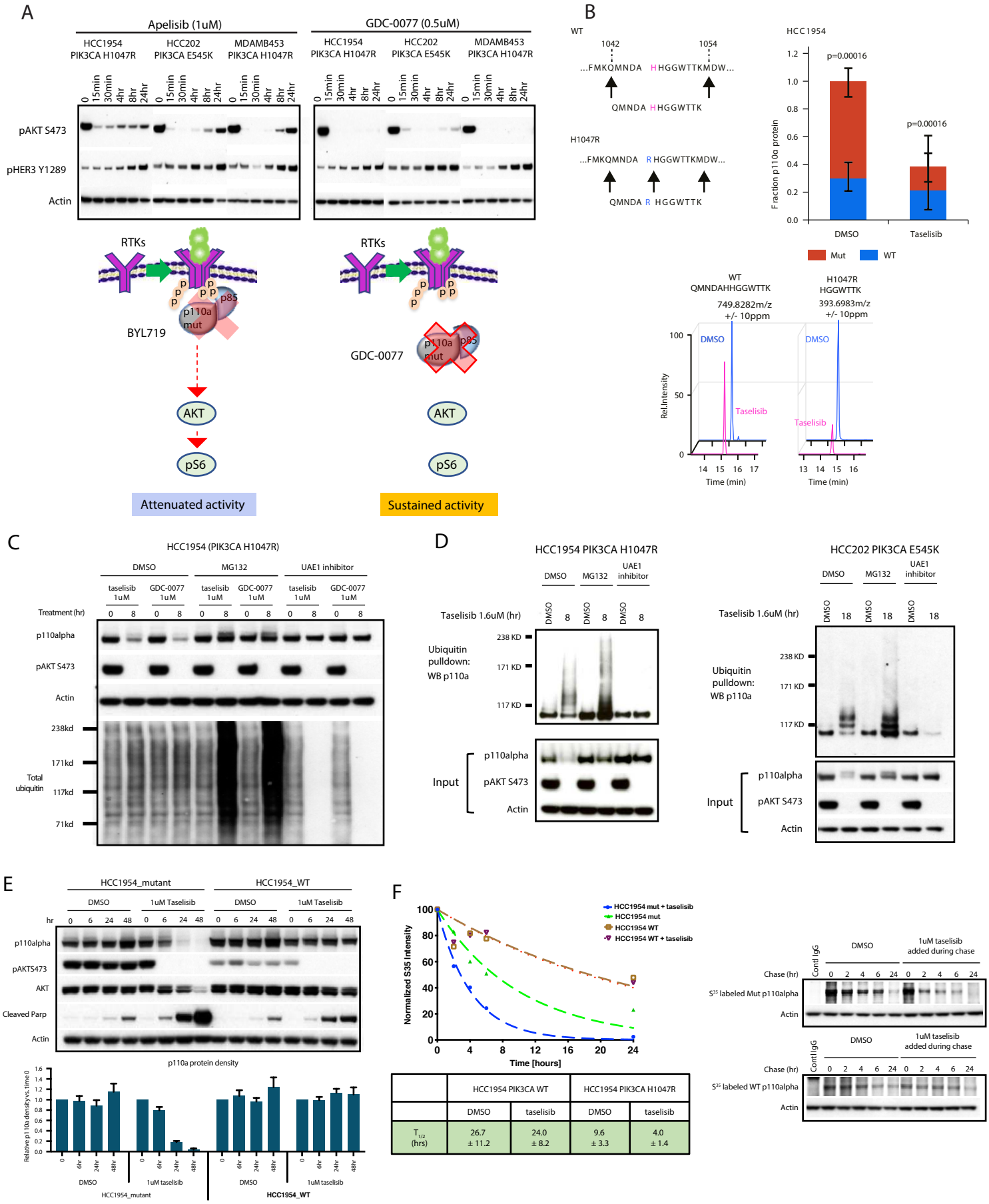

Figure 4

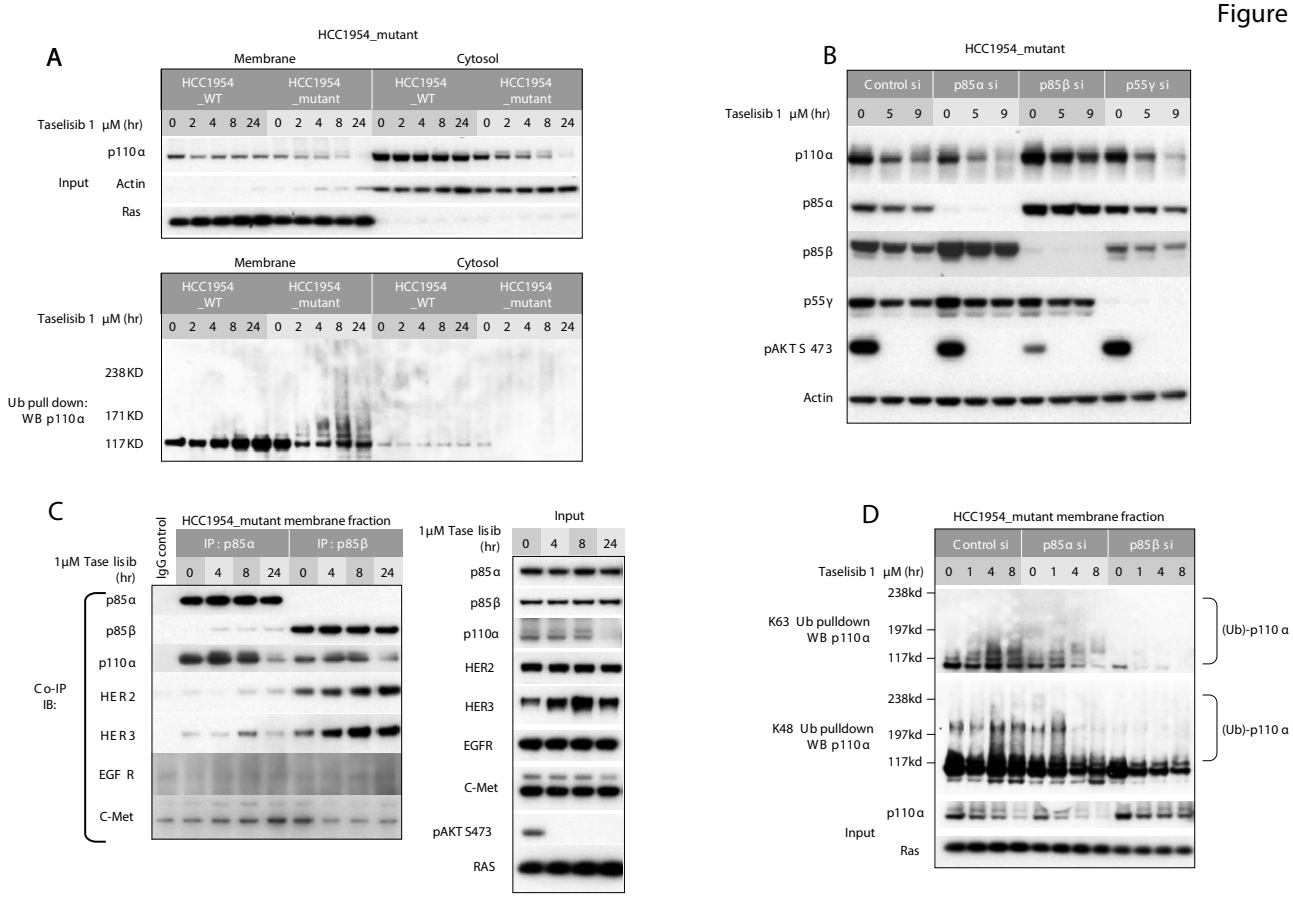

Figure 5

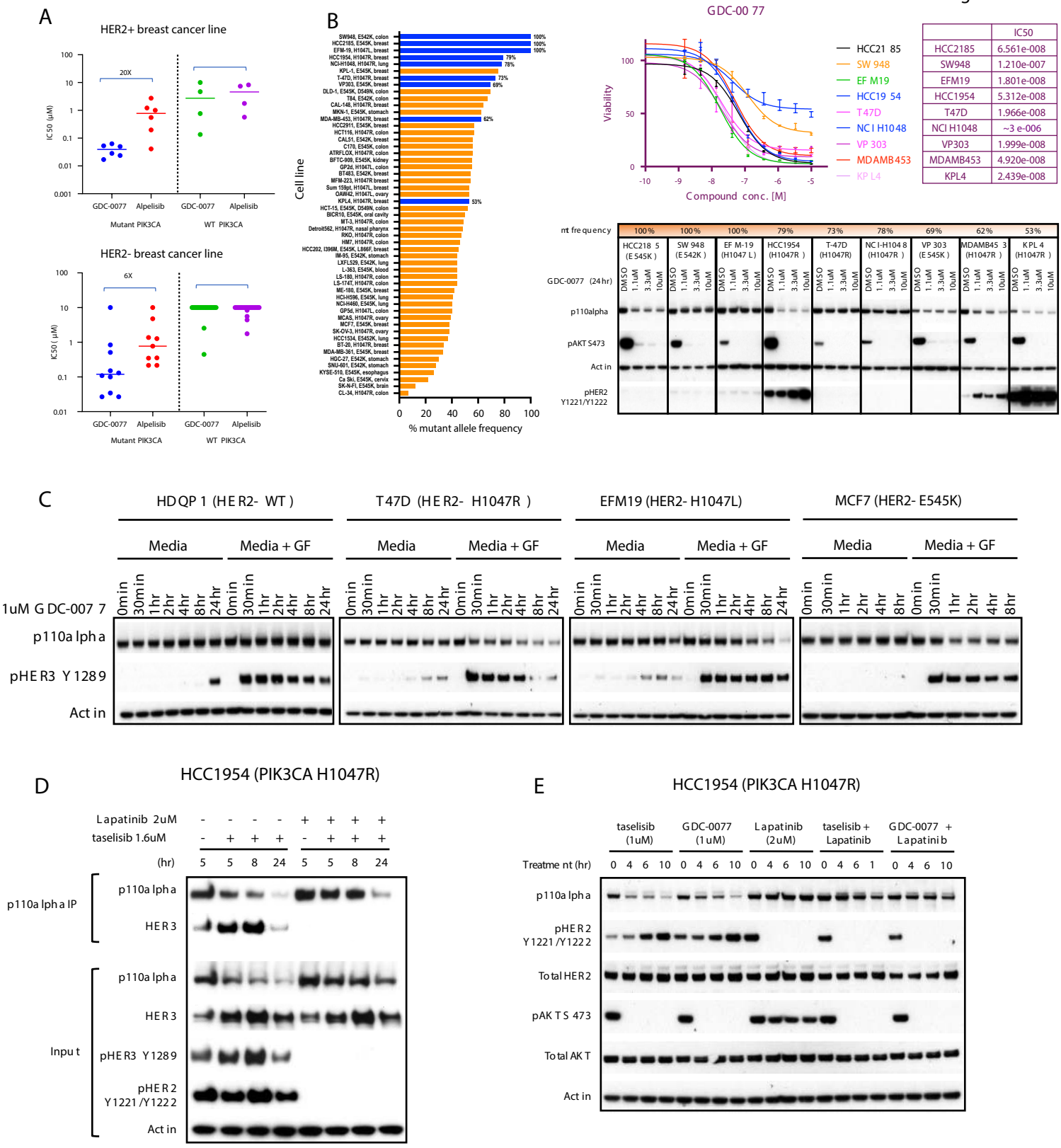

Figure 6

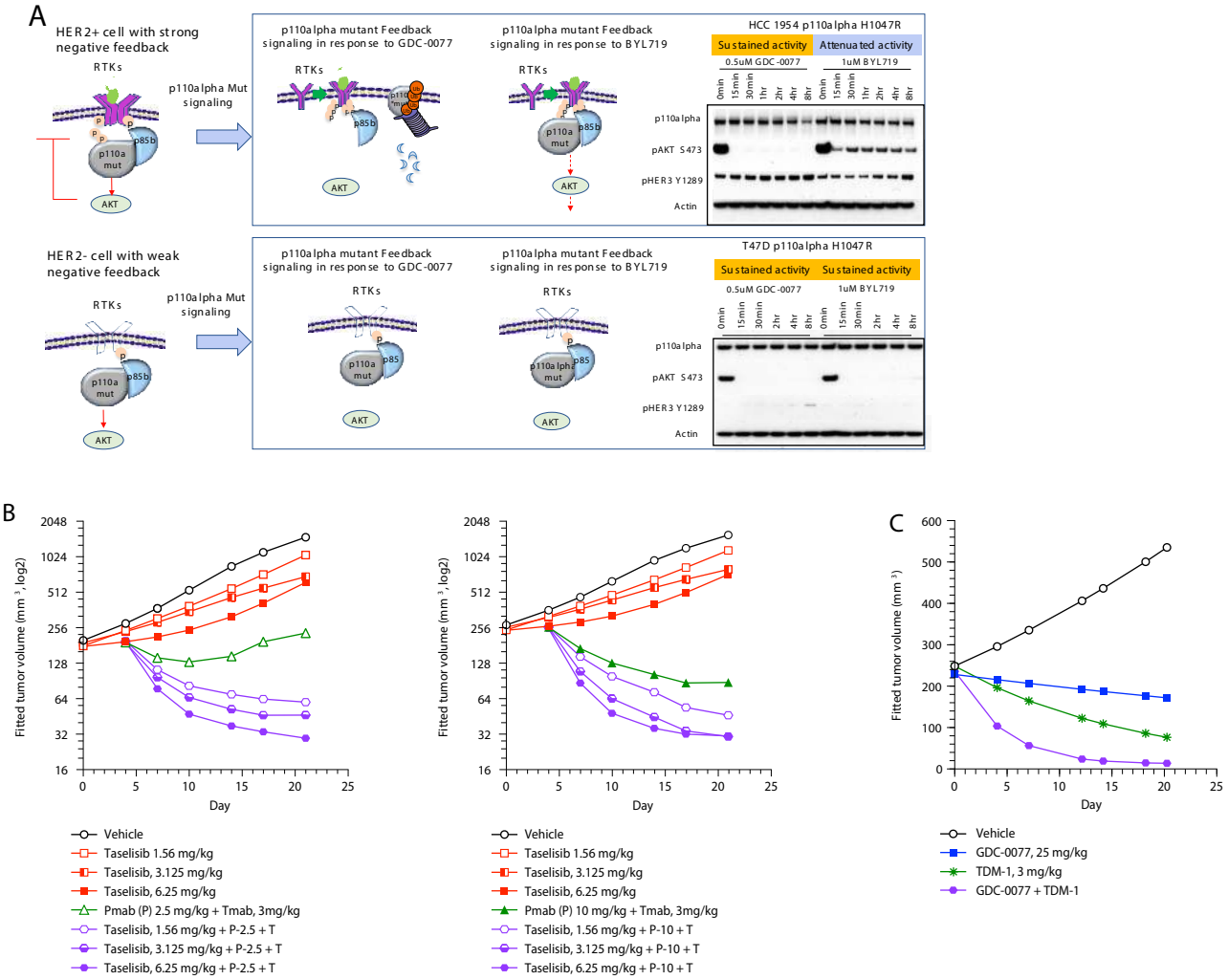

Figure S1

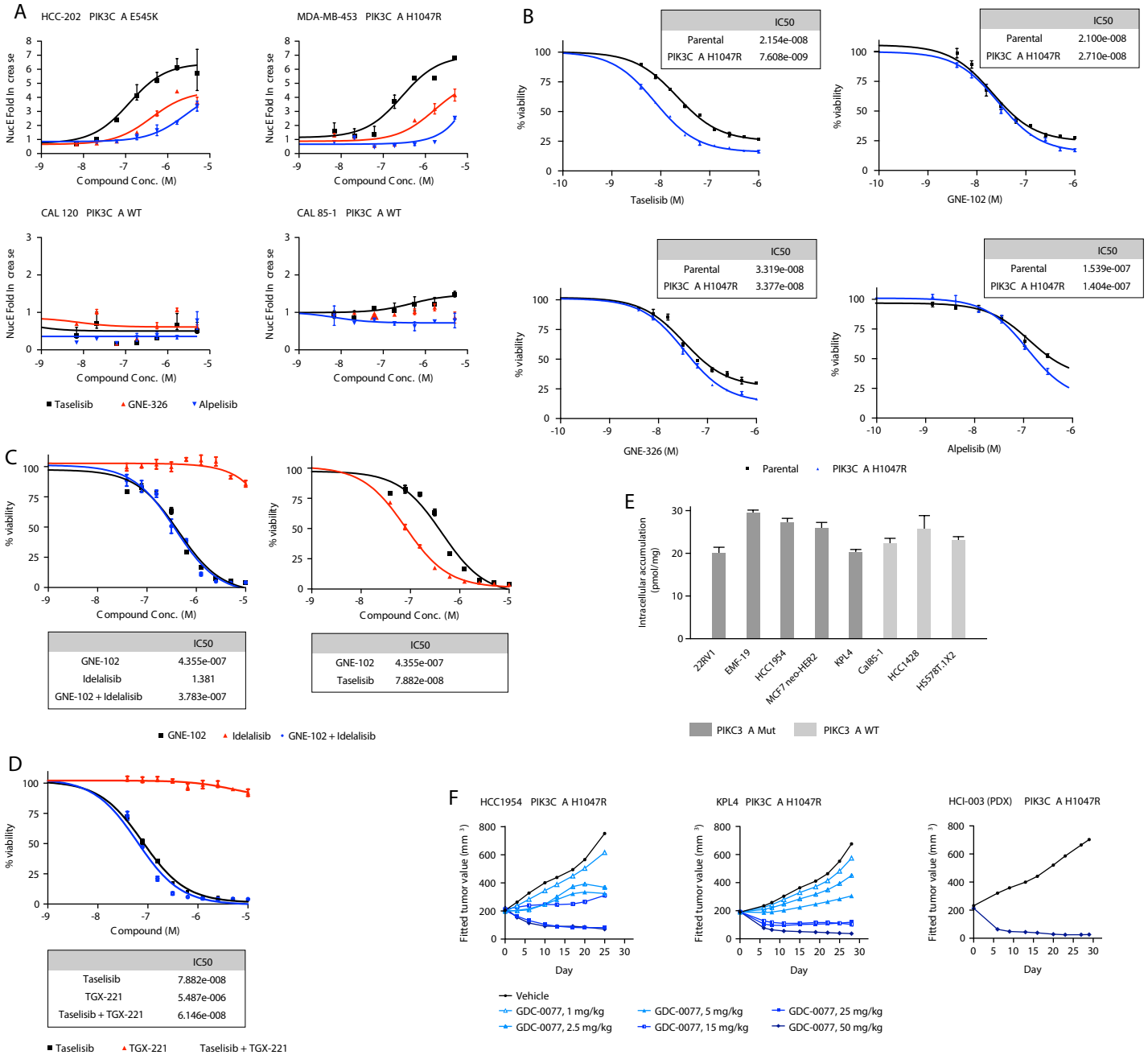

Figure S2

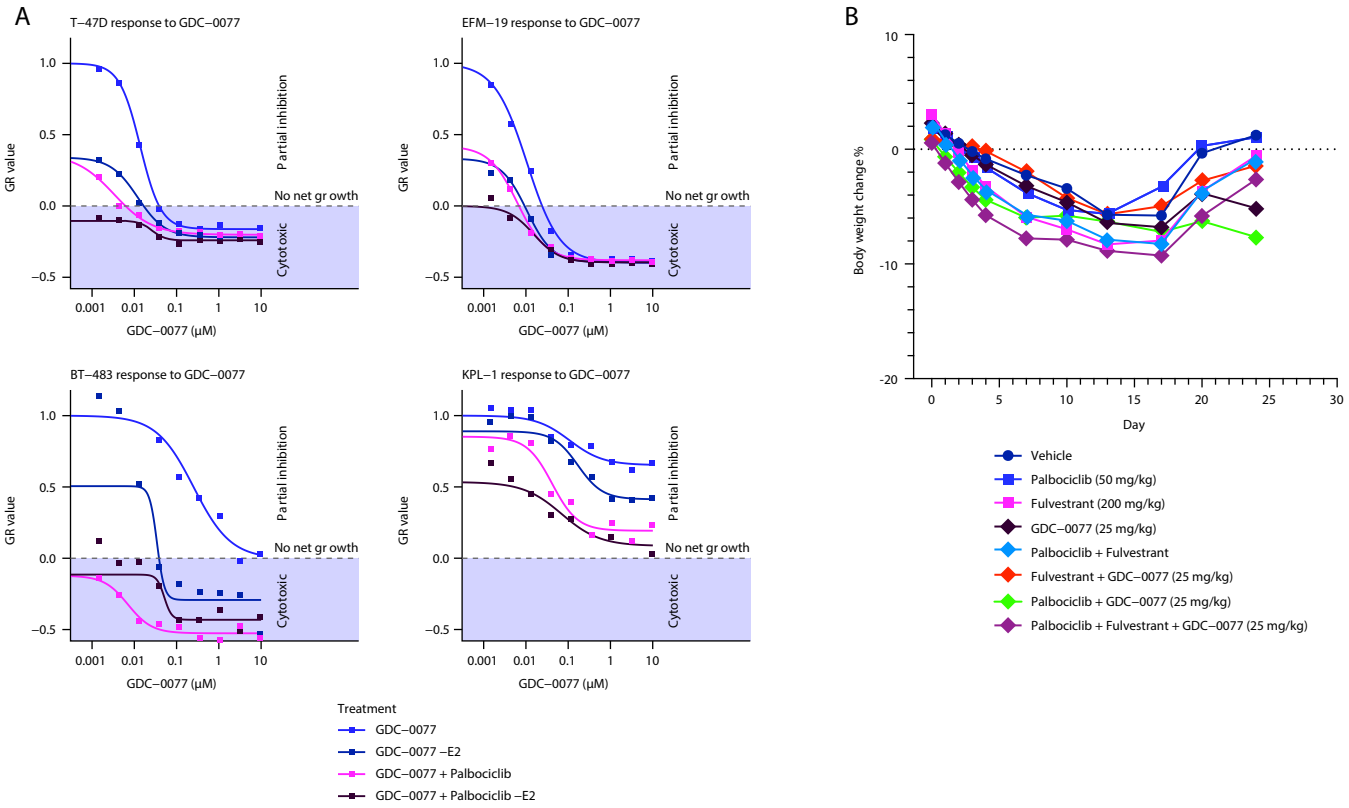

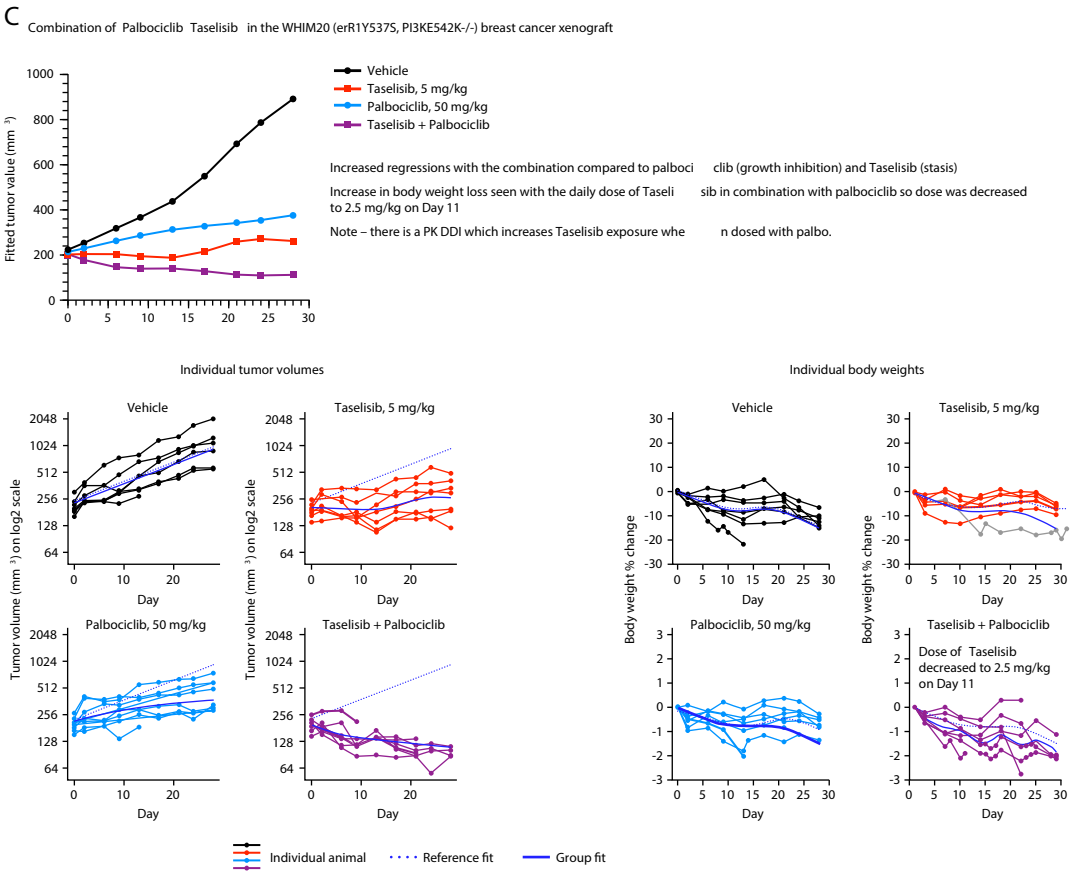

Figure S3

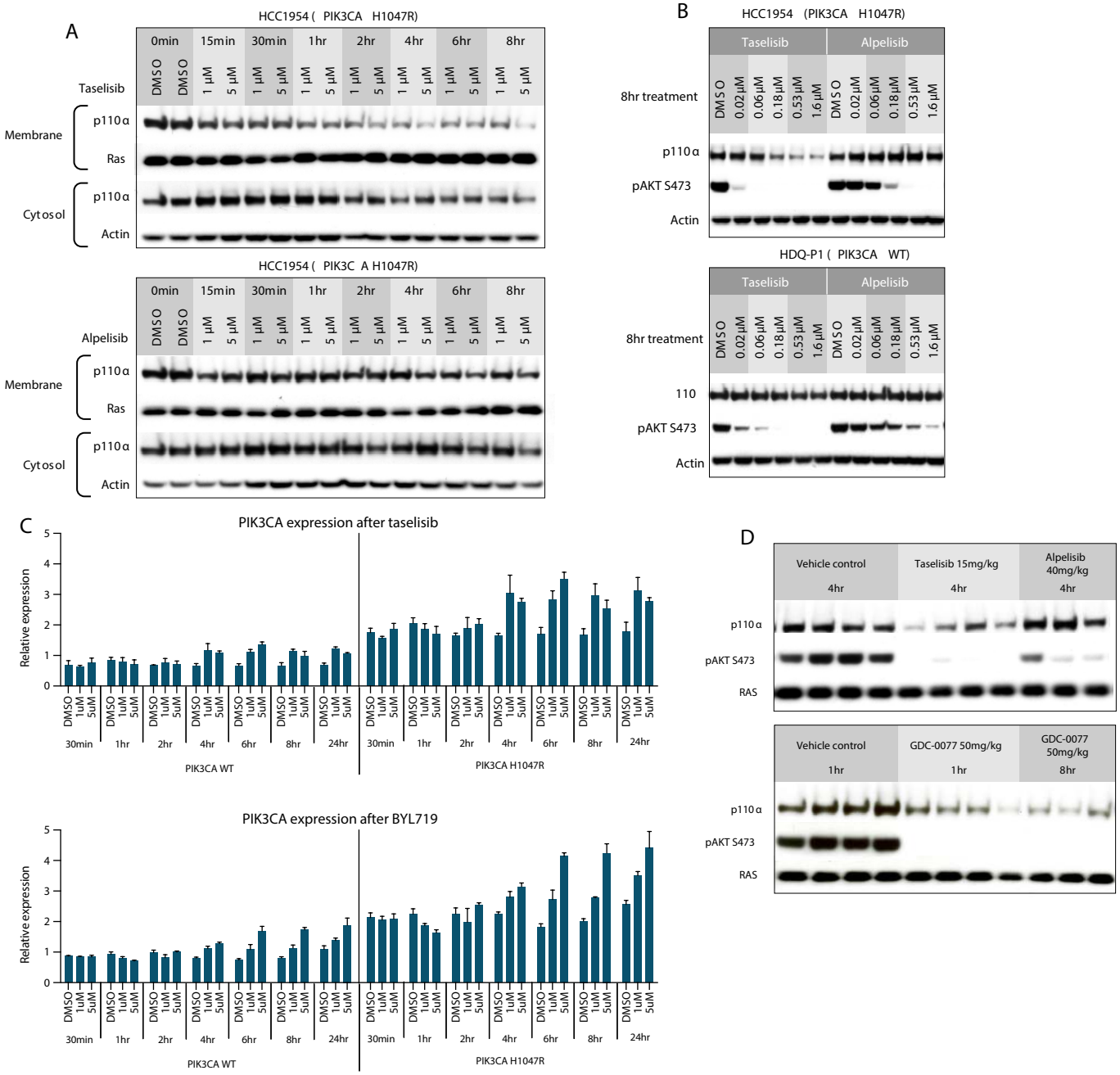

Figure S4

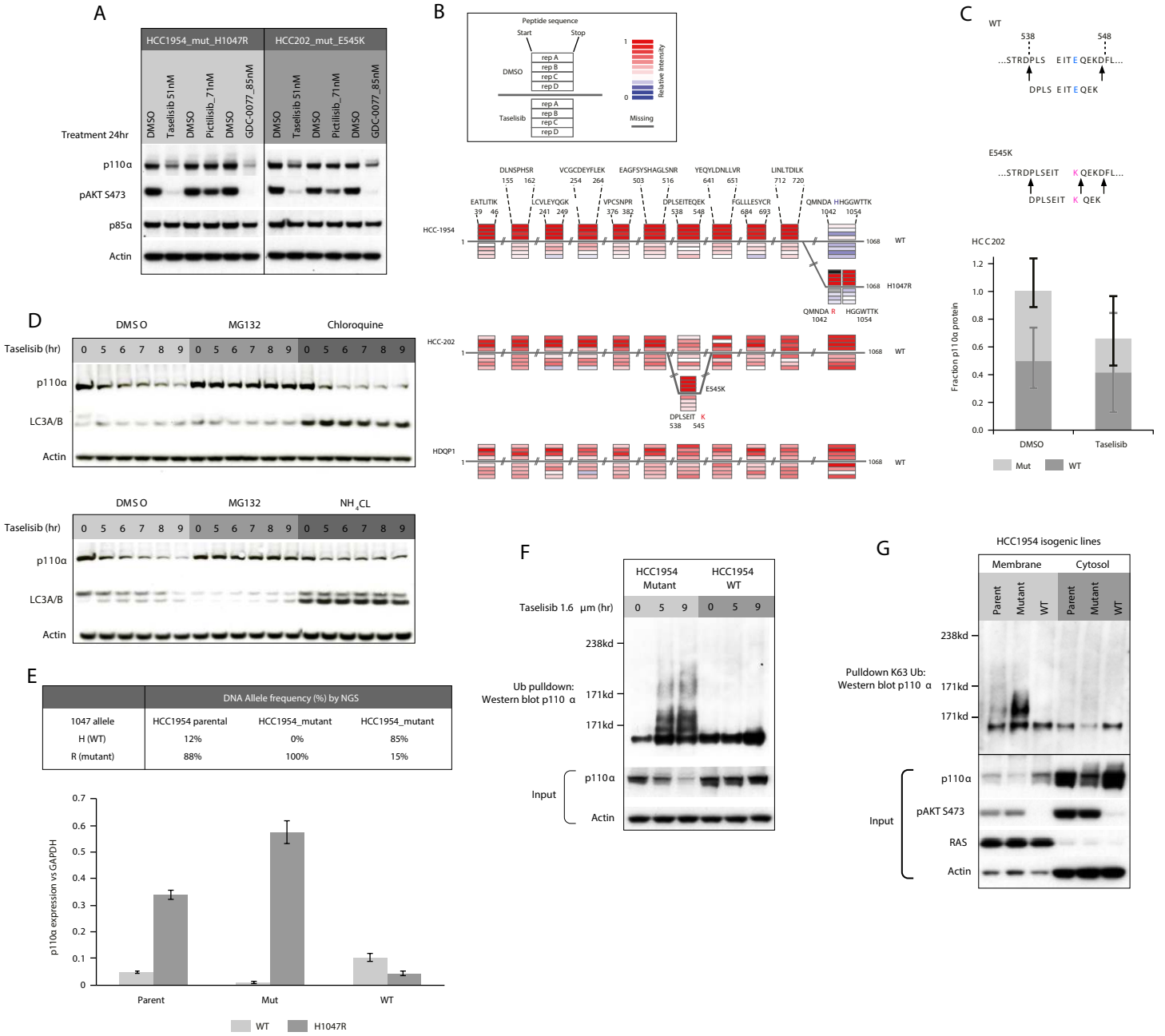

Figure S5

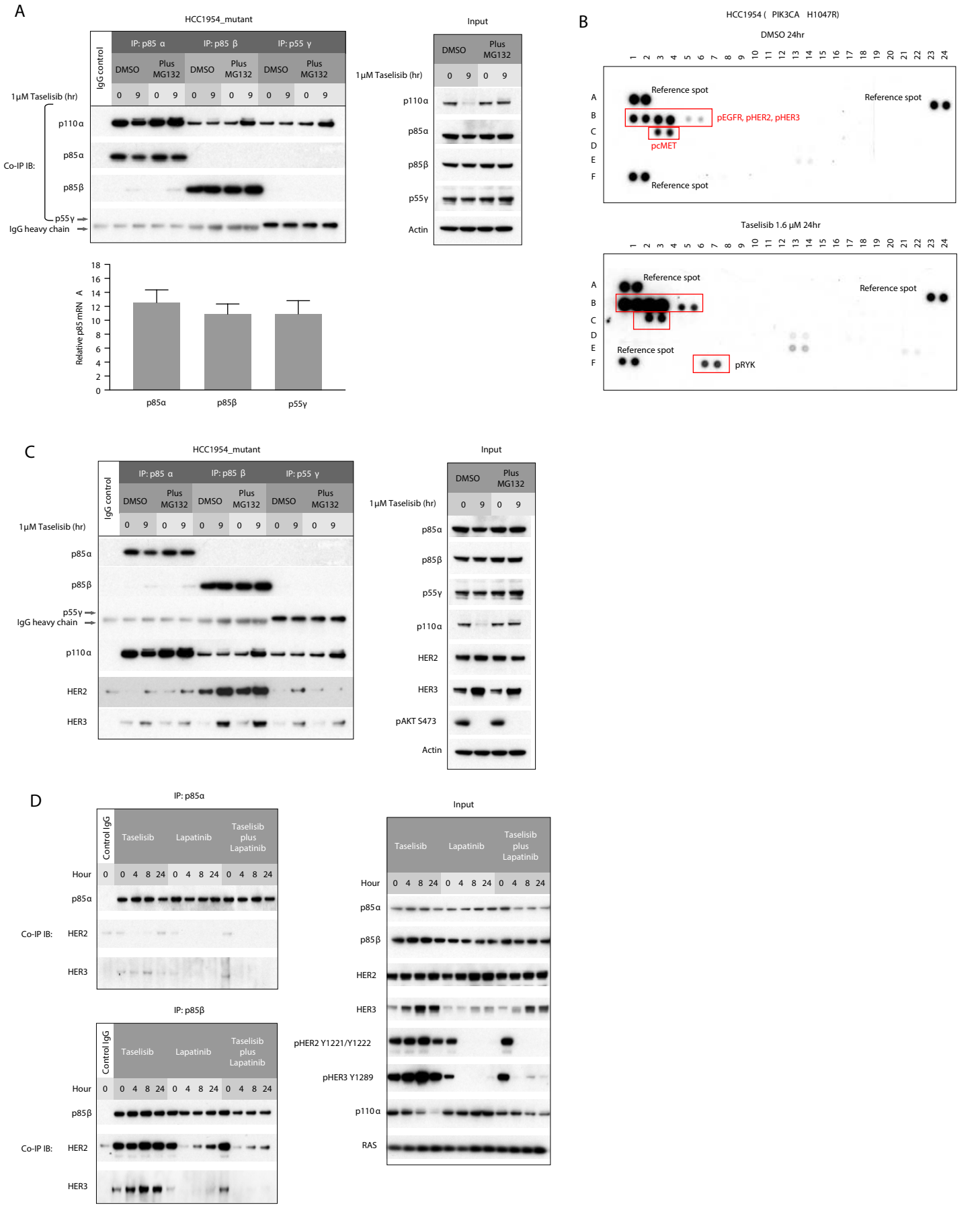

Figure S6